Title
ON THE STABILITY OF PRECIPITATED AUSTENITE AND THE TOUGHNESS OF 9Ni STEEL

Author
Fultz, B.

Publication Date
1984-08-01

LBL-17791
Preprint

Lawrence Berkeley Laboratory
UNIVERSITY OF CALIFORNIA

Materials & Molecular Research Division

Submitted to Metallurgical Transactions

ON THE STABILITY OF PRECIPITATED AUSTENITE AND THE TOUGHNESS OF 9Ni STEEL

B. Fultz, J.I. Kim, Y.H. Kim, H.J. Kim,
G.O. Fior, and J.W. Morris, Jr.

August 1984

Prepared for the U.S. Department of Energy under Contract DE-AC03-76SF00098

DISCLAIMER

ON THE STABILITY OF PRECIPITATED AUSTENITE AND THE TOUGHNESS OF 9Ni STEEL

B. Fultz, J. I. Kim* , Y. H. Kim, H. J. Kim, G. O. Fior and J. W. Morris, Jr.

Materials and Molecular Research Div., Lawrence Berkeley Laboratory,
and the
Dept. of Materials Science and Mineral Engineering,
University of California, Berkeley, CA 94720

ABSTRACT

A correlation was confirmed between the good low temperature Charpy toughness of 9Ni steel and the stability of its precipitated austenite against the martensitic transformation. Changes in the microstructure during isothermal tempering were studied in detail. The austenite/martensite interface is originally quite coherent over ~100 A distances. With further tempering, however, the dislocation structure at the austenite/martensite interface changes, and this change appears to be related to the increased instability of the austenite particles. The strains inherent to the transformation of austenite particles create dislocation structures in the tempered martensite. The energy required to form these dislocation structures affects the thermodynamics of the transformation. Together with a reduction in carbon concentration during tempering, changes in these dislocation structures may also reduce the thermodynamic stability of the austenite particles as they grow larger. The large deterioration of the Charpy toughness of overtempered material is attributed, in part, to these dislocation structures, which resemble the dislocation structures found in cold-worked material.

* IBM Thomas J. Watson Research Center, Yorktown Heights, New York 10598.

I. INTRODUCTION

9Ni steel was developed by the International Nickel Company in 1942 as a ferritic material for cryogenic service [1,2]. After tempering for about one hour at 600°C, 9Ni steel exhibits a beneficial suppression of its ductile-to-brittle transition temperature (DBTT) by more than 100°C. This tempering temperature is within the austenite plus ferrite two-phase region of the equilibrium phase diagram. After tempering, a few percent of austenite (γ-phase) is found between the martensite (α'-phase) laths and along the prior austenite grain boundaries [3-6]. The formation of austenite is the most prominent microstructural change observed after tempering. Furthermore, the presence of austenite is the only clear difference between the microstructure of 9Ni steel and the microstructure of 6Ni steel, for which there is no improvement in DBTT after a simple tempering. It is therefore widely accepted that precipitated austenite can be beneficial to toughness at cryogenic temperatures [7-10]. It is also recognized that the mere presence of austenite is insufficient to ensure this beneficial effect. C. W. Marschall, et al. [7] performed a systematic study of the effects of different tempering treatments on the Charpy toughness of 9Ni steel at 77 K and 290 K. They correlated these toughness data to the amount of austenite present at room temperature, both before and after the material was immersed in liquid nitrogen. In this way they found it necessary for the austenite to be thermally stable against martensitic transformation if good cryogenic toughness is to be obtained. Tempering for much longer than 10 hrs at 600°C, or tempering at higher temperatures, was found to be deleterious to both austenite stability and to cryogenic toughness. Similar systematics have been reported by others [11-14].

Relationships between the stability of austenite and cryogenic fracture toughness have been an important, albeit a controversial topic of research [3-5,7-23]. Early ideas that the soft austenite phase served to blunt a propagating crack, as well as ideas that any fresh untempered martensite near the crack tip will promote brittle fracture, have been ruled out by observations that all austenite transforms to martensite in the plastic zone ahead of the crack tip [3,11,18,19]. A model has been proposed in which the transformation strains associated with the austenite to martensite transformation reduce the strain energy available for crack propagation [23]. It has also been suggested that the austenite serves as an "interstitial scavenger" and promotes a cleaner and more ductile martensite [7]. Kim and Schwartz have suggested that the austenite is helpful as a scavenger until a connected network of austenite has formed in thu material, and then the toughness deteriorates [11].

A transmission electron microscopy (TEM) study of 9Ni steel by Morris, et al. [21,22] has indicated a qualitative difference between the martensite which forms from thermally unstable precipitated austenite and the martensite that forms from thermally stable retained austenite. Thermally unstable austenite particles were found to transform to variants of martensite with a close crystallographic alignment to the surrounding martensite laths. On the other hand, thermally stable austenite particles were found to transform under mechanical loading to those crystallographic variants of martensite compatible with

the applied stress. These martensite particles will usually have a crystallographic orientation different from the common orientation of the neighboring laths. It appeared that the co-operative cleavage of packets of aligned martensite laths was impaired by this transformed austenite. Quasi-cleavage fracture is the low temperature brittle fracture mode, so its impairment should promote more ductile-dimple fracture and better cryogenic toughness.

With so many plausible models, a complete understanding of how the stability of precipitated austenite in 9Ni steel affects mechanical properties will likely remain elusive for the near future. We suggest that further progress requires the examination of one facet of this problem at a time. Accordingly, we have undertaken a modest search for microstructural connections between the loss of austenite stability and a concomitant deterioration of cryogenic toughness that occurs with overtempering of 9Ni steel. The changes in mechanical properties of 9Ni steel that occur during isothermal tempering are large, so a microstructural study of 9Ni steel during isothermal tempering seemed a promising avenue to seek a connection between austenite stability and mechanical behavior.

We have recently completed experimental measurements of changes in Ni, Mn, Cr, and Si concentrations of precipitated austenite during tempering [20,24,25]. These four elements segregate to the austenite and help to stabilize it. The principal change in these concentrations during isothermal tempering was an increase in the Ni concentration (from 12 to 16%), which should help to stabilize the austenite with increased tempering time. Since we show in the present work that the austenite stability decreases with increased tempering time, we have chosen to describe this other work on Ni, Mn, Cr and Si concentrations in a future paper [25].

In the present paper we report results of a microstructural investigation emphasizing the physical properties of the austenite during isothermal tempering. We concentrate on three microstructural changes which correlate to the austenite stability and the low temperature Charpy toughness. These are the carbon concentration of the austenite, the coherency of the austenite/martensite interface, and the dislocation structures created during the transformation of austenite particles. It is suggested that the loss of austenite stability and toughness that occur during tempering have causal relationships with these microstructural changes. These relationships suggest microstructural characteristics that are to be either pursued or avoided if retained austenite is to be associated with good cryogenic toughness.

EXPERIMENTAL PROCEDURES

Commercial 35 mm plates of 9Ni steel with the "QT" heat treatment were kindly supplied by the Nippon Kokan Company. The N.K.K. mill sheet gave the chemical composition listed in Table I, and these data were verified before and after our heat treatments. The as-received microstructure was largely erased, and a fully martensitic microstructure was developed with the heat treatment: (1050^{o}C 3 hrs/ice brine quench) followed by the "Q" treatment: (800^{o}C 1 hr/ice brine quench).

Intercritical tempering was performed at 590°C for times ranging from about 0.8 hrs to 627 hrs, and differing by factors of 3. Standard Charpy bars with crack plane orientation L-S were machined from the centers of the tempered plates.

TABLE I. CHEMICAL COMPOSTION OF 9Ni STEEL (wt.%)

Fe	Ni	Mn	Si	Cr	C	P	S
Bal.	9.1	.50	.20	.17	.08	.004	.004

Cryogenic Charpy tests at temperatures from 160 K to 290 K were performed according to ASTM standards E-23 and A-370 [26] using a bath of ethyl alcohol cooled by liquid nitrogen. A bath of isopentane (2-methylbutane) was used for temperatures from 115 K to 170 K. Health hazards associated with this chemical motivated us to try an alternative procedure for obtaining temperatures from 77 K to about 130 K. Heat was conducted out of the specimens through large aluminum blocks with their lower ends immersed in liquid nitrogen. Specimen temperatures were controlled by the cross sections of the blocks, their lengths, and the shape of the dewars. Although the temperatures of the specimens cooled in this way were inhomogeneous within 7 K at 130 K, the Charpy data were the same as those obtained with the isopentane bath procedure. At least ten specimens with each tempering treatment were used for the data of Fig. 3. Two or three specimens were broken at 77 K and 290 K, but generally only one specimen of each type was broken at each intermediate temperature.

Surfaces for room temperature analysis by x-ray diffractometry (XRD) and by backscatter Mossbauer spectrometry (BMS) were prepared from test sections of the heat-treated plates and from the centers of the undeformed regions of Charpy specimens broken at room temperature. Surface preparation involved sectioning the material with an abrasive saw under flood cooling, a deep grinding on wet silicon carbide papers of 120 to 400 grit, and a deep polishing for 1 to 2 minutes with a fresh solution of 3% HF, 29% H_2O_2 and 68% H_2O. All surfaces had the same orientation with respect to the original rolling direction of the plate, and were always mounted in the x-ray diffractometer with the same orientation. (No significant rolling texture was observed in the tempered materials, however.)

In order to test the mechanical stability of austenite, some of the material was cold rolled at room temperature to a 75% reduction in thickness. Tests of the thermal stability of austenite were performed by immersing the material into a bath of liquid nitrogen. The transformation was athermal. In a test with thin specimens of overtempered material, the same amount of austenite had transformed after liquid nitrogen immersions of <1 sec, 100 sec and 10^5 sec. Our thermal stability test consisted of four thermal cycles. Each cycle included a liquid nitrogen immersion, a 3 min holding in liquid nitrogen, and

finally an immersion in ethanol to warm the specimen to room temperature. The transformation of the austenite occurred mainly after the first cycle; a nearly imperceptible amount of transformation occurred after the third or fourth immersion. After cold rolling or liquid nitrogen immersion, new surfaces were prepared before measuring the remaining amount of austenite.

Thermal expansion measurements were performed with a Theta Industries Dilatronic III dilatometer using a heating rate of 37°C/min and a low backpressure of He gas. In addition to 9Ni steel, a Fe-16Ni alloy, perhaps more representative of the composition of the precipitated austenite, was also used for thermal expansion measurements. Thermal expansion data were taken both below the A_S temperature and above the A_F temperature, so that the difference in thermal expansion coefficients of the austenite and martensite could be determined.

X-ray diffractometry measurements employed a Picker X-ray Inc. diffractometer model 3488K with a parafocussing LiF monochromater. Fe K_α radiation was used to minimize fluorescence of the specimens. The x-ray tube was operated at 7 ma at 40 kV. The diffractometer was run under numerical control and provided a punched paper tape of counts versus 2θ angle for the peaks: (111)γ (110)α′ (200)γ (200)α′ (220)γ (211)α′ (311)γ. The background was measured for at least 2-3° in 2θ angle above and below each peak. These paper tapes were read into a microcomputer system for processing. A linear sloping background was subtracted and the peaks were integrated. The volume fraction of austenite was determined with the method suggested by Miller [27] in which the average of the (220)γ and (311)γ peak intensities is weighted and compared to the (211)α′ peak intensity. Comparison with the Mossbauer spectrometry data for volume fraction of austenite suggested a weighting constant of 1.3 rather than the value of 1.4 offered by Miller for Mo K_α radiation, but the agreement between the XRD and BMS data was otherwise good*. The positioning of the specimens in the diffractometer was not adequately reproducible, so the specimen surface was dusted with NiO powder after each run. The positions of the (111)NiO, (200)NiO and (220)NiO peaks were then used to determine average 2θ corrections for each austenite and martensite peak. These corrected average positions were used to determine the austenite and martensite interplanary spacings.

The broadening of both austenite and martensite x-ray diffraction peaks was analyzed to provide information on the internal strain distributions, and the average size of the coherently diffracting domains. The "method of multiple orders" due to Warren aod Averbach [28-30] could not be used for this analysis because of the large number of specimens involved and the intensity and wavelength limitations of our diffractometer. Instead, the following method was used: A Rachinger correction [31] was performed to remove the $K_{\alpha 2}$ component of each peak. Instrument lineshapes were obtained from a large-grained (50 μm) austenitic specimen of a binary Fe-31Ni alloy annealed at 1100°C and

---

* The difference in Lorentz polarization factors for Mo K_α and Fe K_α radiation suggest changing Miller's weighting constant to 1.25 for Fe K_α radiation.

furnace cooled over a period of 4 hrs. Appropriate instrument lineshapes were then deconvolved [32] from each peak with a fast Fourier transform method. The statistical scatter in the experimental data contributed excessive amplitude to the higher order Fourier coefficients. To prevent divergence of the inverse Fourier transform, the transform of the peak divided by the transform of the instrument lineshape was multiplied by a Gaussian function to smoothly suppress the high order coefficients.

In a **Data Analysis** section we show why diffraction peaks from a distribution of small crystals tend to have a Lorentzian profile. Strain distributions in polycrystalline metals have been successfully described by Gaussian functions [28-30]. In general, we expect the presence of both small diffracting domains and an internal strain distribution so we expect a diffraction profile that is the convolution of a Lorentzian function and a Gaussian function. The tails of a Lorentzian function are much stronger ($\sim 1/x^2$) than the tails of a Gaussian function ($\sim \exp -x^2$). Therefore, in separating size broadening from strain broadening, the Rachinger and Stokes-corrected peaks were fit to a numerical convolution of Gaussian and Lorentzian functions, with emphasis on the quality of fit in the tail regions of the peak. The data of Fig. 1 illustrate the method. Peak "a" was resolved into 65% Gaussian and 35% Lorentzian components, peak "b" was 25% Gaussian and 75% Lorentzian, and peak "c" was 10% Gaussian and 90% Lorentzian. We estimate the error in these assignments to be $\pm$5%, to which we add an uncertainty in the total width of the corrected peak in order to estimate the total error in the strain and size broadening data.

^{57}Fe Mossbauer spectra were obtained with a constant acceleration spectrometer using an Austin Science Associates S-600 Doppler drive. The drive was synchronized to the clock of a microcomputer that served as a multichannel scaler [33]. Room temperature spectra from 14.4 keV γ-rays were obtained with a backscatter detector of recent design [34]. Transmission Mossbauer spectrometry (TMS) was used for collecting 14.4 keV Mossbauer spectra at high temperatures. An evacuated tube furnace with good temperature homogeneity was installed on the Mossbauer spectrometer. Thin specimens for the TMS experiments were cut directly from the Q treated plates, and polished to approximately 40 μm with the 3% HF solution. A series of temperings at 600°C were performed in the evacuated tube furnace. After each tempering, the temperature was reduced to 500°C to permit the collection of a Mossbauer spectrum without the concurrent formation of more austenite. The amount of austenite measured in this way was representative of the amount that had actually formed at 600°C. For some specimens the furnace was turned off so that the amount of austenite that transformed upon cooling to room temperature could be determined.

The central part of a backscatter Mossbauer spectrum from overtempered material is shown in Fig. 2. The integrated intensity of the central austenite peak was corrected for overlap of the tails of the two $\pm 1/2 \rightarrow \mp 1/2$ martensite peaks by stripping Lorentzian functions characteristic of these two peaks from the spectrum (see crosses in Fig. 2). The atomic fraction of austenite was determined from the ratio of intensity of the austenite peak to the integrated intensity of the entire spectrum.

Integrated peak intensities were given approximate corrections for the thickness distortion inherent in spectra from BMS [35] and TMS [37]. These data were converted to volume fraction of austenite by assuming an 80 at.% concentration of Fe in the austenite.

Specimens for study by TEM were first cut into wafers of 400 μm thickness by an abrasive wheel saw with flood cooling. These wafers were thinned to 100 μm in a solution of 3% HF, 29% H_2O_2 and 68% H_2O. The chemically-thinned wafers were spark-cut into disks of 3 mm diameter, which were ground on a set of SiC papers to a thickness of 50 μm. These disks were thinned to perforation in a twin-jet electropolishing apparatus using a cooled solution of 400 ml CH_3COOH, 75 gm CrO_2 and 30 ml H_2O. These foils were examined with Phillips 301 and Phillips 400ST electron microscopes operated at 100 kV and 120 kV, respectively. Moiré fringes from the austenite/martensite interface were obtained in bright field micrographs with the (333)γ and the (330)α′ diffractions operating strongly. High index diffracting planes were used for Moiré fringes because the interplanary spacings of (111)γ and (110)α′ are so similar that only a few fringes could be seen across small austenite particles. Lattice images of the austenite interface were obtained from a through focus series taken with the two beam tilted illumination method. The diffracted beams from the (111)γ and (110)α′ planes were combined with the transmitted beam for image formation.

II. DATA ANALYSIS AND RESULTS

General Microstructural Changes During Tempering

Figure 6 shows how the amount of austenite depends on tempering time. The austenite content was measured with four sets of experimental conditions: 1) at 500°C after tempering at 600°C, 2) at 17°C after the quench to 0°C, 3) again at 17°C after four thermal cycles between 17°C and 77 K, and 4) after 75% cold rolling at 17°C. The amount of austenite that remained after the cold-rolled material was immersed in liquid nitrogen was only slightly less than the amount that remained after cold rolling alone. The amount of austenite present in the foils used for TMS experiments at 500°C after tempering at 600°C was a few percent less than the amount that was present in the furnace-treated plates, so the 500°C data in Fig. 6 show the difference between the amount of austenite in the foil at 500°C and at room temperature. The amount of austenite in material that was tempered for more than 100 hrs had poor reproducibility, even for specimens that were heat treated in the same batch (see the scatter of the data for one batch of 300 hr tempered material in Fig. 6). This variability reflects differences in the amount of transformation that occurs during the quench from 590°C to 0°C. In particular, less austenite was found after quenching small bars of this overtempered material, and we suspect that higher cooling states are responsible for more transformation of the austenite. We did not find such a large variation for the amounts of austenite in materials tempered for less than 100 hrs; these amounts were reproducible to ±1% for different batches of material prepared in the same way.

The austenite is most stable after short tempering times; after 3 hrs of tempering the austenite is thermally stable and has good mechanical stability. The austenite begins to lose mechanical stability after a few hours of tempering, and the fraction of austenite that transforms during cold rolling continues to increase with tempering time. The M_S temperature for the precipitated austenite increases from below 77 K to room temperature after about 50 hrs of tempering, and the austenite is quite thermally unstable after 100 hrs of tempering. These continuous systematics suggest that the distinction between thermal stability and mechanical stability is a distinction primarily in the degree of stability. Thermal stability and mechanical stability do not seem to be intrinsically different.

The TEM micrographs of Figs. 7-9 show that as tempering proceeds it is the growth of the existing austenite particles, rather than a continuing nucleation of new particles, that is responsible for the increasing amount of austenite shown in Fig. 6. Some particles of austenite are labeled with the letter "a", and the letter "f" (for ferrite) is superimposed on the tempered martensite matrix. All dark field micrographs were taken with an isolated $00\bar{2}\gamma$ diffraction from a diffraction pattern in which the $\langle\bar{1}11\rangle\alpha'$ and $\langle\bar{1}10\rangle\gamma$ zone axes were coincident. To within a few degrees, these diffraction patterns showed that the austenite and the martensite obey the Kurdjumov-Sachs orientation relationship [37]: $(111)\gamma \parallel (110)\alpha'$ and $\langle\bar{1}10\rangle\gamma \parallel \langle\bar{1}11\rangle\alpha'$, as previously found for 9Ni and 6Ni steel [3,17,20-23,38].

Some remaining austenite is seen in the dark field image of Fig. 9. However, material tempered for 240 hrs shows dark and dislocated regions with the shape of retained austenite particles in the bright field micrograph. These regions, labeled with a "m" were shown by selected area diffraction to have a bcc structure with the same crystallographic orientation as the neighboring laths. We identify these regions as fresh, untempered martensite particles that formed during the quench from 590°C to 0°C. Some of the austenite transformed to fresh martensite particles during preparation of the foil specimens for TEM. In material tempered for 81 hrs, there appeared to be as many fresh martensite particles as austenite particles in the TEM specimens, even though Fig. 6 shows that little austenite had transformed in the bulk material.

Tempering induces recovery of the martensite matrix. The recovery of the martensite is fairly complete after 9 hrs of tempering at 590°C, except for local regions with crisply resolved defect structures. The martensite matrix looks rather clean after 81 hrs of tempering (Fig. 8). However, two new features are seen around the fresh martensite in material tempered for 240 hrs (Fig. 9). One new feature is a mottled gray layer that surrounds the top of the fresh martensite particle in the center of Fig. 9. This cloudy electron contrast is not uniformly distributed; for example, it does not extend to the bottom of the particle. The second new feature consists of dark lines that radiate outwards into the tempered martensite from the fresh martensite particle; the letter "f" in Fig. 9 covers a few such lines. Untransformed austenite particles in material tempered for 300 hrs are seen in Fig. 10. Especially around the ends of these austenite particles, localized strains cause

loops of dark contrast to appear in the image of the martensite matrix (Fig. 10a).

Higher magnification TEM micrographs are shown in Figs. 11-15. Austenite, tempered martensite, and fresh martensite particles are labeled with the letters "A", "F", and "M", respectively. In Fig. 11, an austenite particle from material tempered for 9 hrs has an array of dislocations near the austenite/martensite interface. The dislocations, seen as light and dark lines running across the thickness fringes, have a semi-regular spacing of about 100 A. In Fig. 13 from material tempered for 81 hrs, a much higher density of dislocations is present near the austenite/martensite interface.

Figure 13 shows fresh martensite and tempered martensite in material that was tempered for 240 hrs. Thick rough lines originate at the fresh martensite and traverse the tempered martensite. Some of these lines moved under electron irradiation. The cloudy gray contrast in Fig. 9 appears in the higher resolution image of Fig. 13 as a dense entanglement of dislocations covering some, but not all, of the fresh martensite particles. Some micro-twinning, designated by a "T", is seen in the fresh martensite. Occasionally a Fe_3C particle was found in the material tempered for a long time. One such particle is identified by selected area diffraction in the dark-field image of Fig. 13. Fig. 14 shows the dislocation structure around fresh martensite particles in material tempered for 300 hrs. The austenite particles were not completely transformed to martensite, and the transformation shows some tendency to occur in the center of the particles. The dislocations around the particles appear to be forming into dislocation walls, but this process is incomplete. A smaller fresh martensite particle from 81 hr tempered material is shown in Fig. 15. The dense mesh of dislocations near the surface of the particle is present, but there is little disturbance of the tempered martensite away from the particle. A bright field TEM micrograph of material tempered for 3 hr and then given 25% cold work is shown in Fig. 16. A dense dislocation structure is seen around a martensite lath in the upper left corner of the figure, and a partially-formed dislocation wall structure is seen in the lower right.

Carbon Concentrations

There have been many suggestions that the segregation of carbon to precipitated austenite is a major factor in determining the stability of the austenite. Unfortunately, measurements of the partitioning of small amounts of carbon between the austenite and martensite are unfeasible with most techniques for chemical analysis. Here, we determine the carbon concentration of the austenite by analyzing x-ray lattice parameters. First we analyze the martensite lattice parameter in conjunction with measurements of the amount of austenite which had formed, and second we analyze the austenite lattice parameter directly.

Particle size effects broaden an x-ray peak symmetrically about its center, so small changes in carbon concentrations (which affect the mean positions of x-ray peaks) can still be determined independently. However, changes in internal strains of austenite and martensite will interfere with the determinations of carbon concentrations from analysis

of lattice parameters. Large microstructural changes are observed in overtempered or cold-worked material when some of the austenite transforms to martensite. In these materials the abrupt shifts in positions of austenite x-ray peaks are largely attributed to transformation-induced changes in elastic strains. Fortunately, no transformation occurred in material tempered for less than 100 hrs, and its microstructure observed by TEM showed no changes from which we should expect strain changes. Consequently, we believe that lattice parameter changes for the first 100 hrs of tempering are largely due to carbon segregation to the austenite. Furthermore, as shown below, analyses of changes in both the austenite and martensite lattice parameters gave mutually consistent carbon segregation data for the first 100 hrs of tempering.

We begin with an analysis of the martensite lattice parameter (Fig. 17). We assumed that the effects of solutes follow Vegard's law over the small ranges of composition that are involved, and assumed that the effects of different solutes are additive. For the chemical composition of martensite, we used the concentrations in Table I for all elements except carbon, which was left as a variable. Then with data of solute effects on martensite lattice parameters compiled by Pearson [39], a 0.04 wt.% carbon concentration for the martensite of 1 hr tempered material was determined. This apparent 0.04% carbon concentration is too low if carbon segregation from the martensite to the austenite is responsible for the further reductions in martensite lattice parameter.

Assuming that each 0.01 wt.% reduction in carbon concentration causes the average martensite lattice parameter to decrease by 0.0003 A, the martensite carbon concentration is reduced by about 0.08 wt.% between 1 and 81 hrs of tempering, with most of this change occurring in the first 10 hrs of tempering. These data suggest that most of the carbon in the material has segregated to the austenite after 10 hrs of tempering. Together with the data of Fig. 7, a steady 0.7 wt.% carbon concentration is found for the austenite during the first 10 hrs of tempering, but this is diluted to about 0.4 wt.% after 81 hrs of tempering. An initial carbon concentration of 0.7% is higher than the 0.1-0.2% concentration obtained from the ternary Fe-Ni-C equilibrium phase diagram estimated by Romig and Goldstein [40]. However, the data of Strife and Passoja [14] suggest that only 5% austenite served to getter most of the carbon in 9Ni steel after tempering for 1 hr at 590°C, implying an austenite carbon concentration of greater than 1%.

If all of the precipitated austenite is transformed into fresh martensite, all the carbon in the material will be in the martensite phase. Since the martensite lattice parameter depends linearly on the carbon concentration, the partitioning of carbon between the fresh martensite and the tempered martensite will have no effect on the average martensite lattice parameter. So if all of the austenite were transformed, our new mixed martensite will have the same lattice parameter as did the martensite before tempering. We therefore attribute the increase in martensite lattice parameter after cold rolling (Fig. 17) in part to the presence of fresh martensite with a high carbon concentration.

We now estimate the austenite carbon concentration by direct analysis of austenite lattice parameters (Fig. 18.) The austenite particles are enriched in solute elements and have a composition*. Fe-16Ni-3Mn-1Cr-XC (in wt.%). Using the lattice parameter of 1 hr tempered austenite together with Vegard's law and data from Pearson for bulk, equilibrium austenite [39], we find an austenite carbon concentration of 0.5 wt.%. It has been previously noted that the lattice parameters of retained austenites tend to be smaller than the lattice parameters of equilibrium austenites [41]. These data for retained austenites in a fresh martensite matrix suggest that our austenite has a carbon concentration between 0.6% [43] and 0.9% [41].

We believe that the changes in carbon concentration of the austenite that occur during tempering can be determined more accurately than absolute carbon concentrations. Assuming that the austenite lattice parameter is reduced by 0.035 A for each reduction of 1 wt.% in carbon concentration, between 1 hr and 81 hrs of tempering the reduction in austenite lattice parameter (Fig. 18) is consistent with a reduction in carbon concentration of 0.3 wt.%. It appears that this austenite lattice parameter reduction is larger between 10 and 100 hrs than between 1 and 10 hrs of tempering, again supporting the idea of Marschall, et al. [7] that the austenite carbon concentration is more steady at first, but becomes diluted after a large amount of austenite has formed. The data of Fig. 18 are in excellent agreement with data reported by Marschall, et al. [7] for the first 100 hrs of tempering at 593°C. Including the composition difference between our material and theirs, agreement is within expected experimental error.

Abrupt Reduction in Austenite Lattice Parameter

The lattice parameter of the austenite in material tempered for more than 100 hrs is 0.5% less than that of material tempered for shorter times. This decrease could be due in part to the dilution of carbon in the austenite. However, there are four reasons why we believe that this 0.5% reduction in austenite lattice parameter must be primarily due instead to increased compressive strains caused by the thermal transformation of austenite. 1) The lattice parameter reduction occurs abruptly between 81 hrs and 243 hrs of tempering, but Fig. 6 suggests that the volume fraction of austenite does not increase by nearly the amount compatible with the required dilution of carbon. (The small amount of Fe_3C detected only with TEM accounts for an insignificant amount of carbon.) 2) The martensite lattice parameter did not show the complementary increase expected if much carbon returned to the martensite phase. The average martensite lattice parameter may even be reduced slightly after 100 hrs of tempering. 3) Similarly large reductions in austenite lattice parameter were observed in cold-rolled material that was tempered for only a short time. In this case the large

---

* We have measured the solute segregation to the austenite by analytical electron microscopy and by Mossbauer spectrometry, and have found approximately this composition [25]. The expected errors in Ni, Mn, and Cr concentration can account for only insignificant errors in the predicted lattice parameter.

lattice parameter reductions must be consequences of strain effects, and not carbon redistributions. 4) The material of Marschall, et al. [7] had formed enough austenite after 700 hrs of tempering at 593°C for a comparable dilution of the austenite carbon concentration. However, the austenite in their material was relatively stable upon quenching to room temperature, and no large reduction in austenite lattice parameter was observed. Marschall, et al. did report such a reduction for material tempered at 621°C in which the austenite became thermally unstable.

It was found that an abrupt reduction in austenite lattice parameter could be induced by other thermomechanical treatments when these treatments caused some austenite to transform to martensite. Cold rolling the material tempered for less than 100 hrs increased the atomic volume difference between the martensite and the remaining austenite from 2.0% to 3.5%. Liquid nitrogen immersion also reduced the lattice parameter of the austenite when the austenite was thermally unstable. The austenite in the overtempered material had a small atomic volume (3.0% less than martensite) that became even smaller after liquid nitrogen immersion (3.9% less than martensite).

Austenite/Martensite Interface

The lattice parameter data for material tempered for 1 to 100 hrs show that the $(111)\gamma$ planes are 2.2% too far apart to match the $(110)\alpha'$ planes. This is based on an average lattice parameter from polycrystalline material, but the narrow widths of the XRD peaks do not allow for a tetragonal distortion to permit matching between one pair of these planes at the expense of a more severe mismatch of the other pairs. The 33 A spacing of the third order Moiré fringes seen in Fig. 19 for 3 hr tempered material is also consistent with a 2.1% mismatch between the $(111)\gamma$ and $(110)\alpha'$ planes. To account for this mismatch, an extra $(\bar{1}10)\alpha'$ plane is required every 100 A along the interface in the $[\bar{1}10]\alpha' = [\bar{1}11]\gamma$ direction. Because they are appropriately separated, we interpret the dislocations at the surface of the austenite particle in Fig. 11 as interface dislocations. Similar interface dislocation structures were observed at austenite particles in other material tempered for less than 10 hrs. Our measurements of thermal expansion suggest that at 600°C the atomic plane mismatch between the austenite and the martensite will be even worse than at room temperature by 0.5%. The interface dislocations were required at 600°C as the austenite was forming, and remain mostly undisturbed when matermal tempered less than 100 hrs is quenched to room temperature. The terminating Moiré fringes indicated by the three open arrows in Fig. 19 suggest the presence of conventional bulk dislocations in either the austenite or the martensite.

The simultaneous imaging of lattice fringes from both $(111)\gamma$ and $(110)\alpha'$ planes from 3 hr tempered material (Fig. 20) shows the high degree of coherency at the austenite/martensite interface. The consistency in contrast of the fringes as they pass through the interface suggests the precision of crystallographic registry across the interface. The straightness of the fringes is a consequence of the accurate parallelism between the $(111)\gamma$ and the $(110)\alpha'$ planes. A precise

delineation of the interface in Fig. 20 is not possible. Nevertheless, one extra fringe from the martensite is seen near the middle of the figure. Since the fringes adjacent to this terminating fringe are continuous through the interface, we interpret the termination of the extra martensite fringe as an interface dislocation that is nearly parallel to the incident electron beam. The Burgers vector associated with the unmatched (110)α' plane could, by geometry, be as small as a pure edge dislocation with a Burgers vector of $1/2a[110]\alpha' = 1/3a[111]\gamma$. However, we expect the energetics of atomic misfit to favor an additional screw component that will tilt the Burgers vector towards $1/2a[111]\alpha' = 1/2a[011]\gamma$, which is a lattice invariant translation of both fcc and bcc lattices. Either the pure edge dislocation or the mixed dislocation could move in the plane of the interface in Fig. 20 in a mostly conservative manner. The latter Burgers vector for interface dislocations was observed by Sandvik and Wayman [43], but their dislocations had pure screw character on a microscopic scale. Their interface dislocations were more regularly arranged than those in Fig. 11, but their mean spacing was comparable. These differences presumably arise because the interface dislocations in their material were generated during the formation of martensite by a crystallographic shear mechanism, instead of during the formation of austenite by a diffusional process.

Theory of XRD Peak Shapes

An analysis of the shapes of x-ray diffraction peaks in terms of a convolution of Gaussian and Lorentzian functions was previously performed by Pines and Sirenko [44]. Although they worked with Fourier transforms of the peaks instead of direct curve fittings as in the present work, they also assigned effects of strain and size broadening to Gaussian and Lorentzian components, respectively. This method can be criticized for assuming the distribution of strains to be the same for all sizes of particles [45]. This assumption will start to cause errors when the asymmetry of the corrected diffraction profile is as large as is seen in Fig. 1c. Fortunately, the asymmetry of Fig. 1c was stronger than that of any other diffraction profile.

The origin of the Lorentzian tails in x-ray diffraction lineshapes results from the distribution of small domain sizes in a manner similar to that proposed by Khachaturyan [47]. His argument is cased on the probability, $P(\ell)$, of not finding a boundary to a column of atomic planes up to the distance, ℓ, where the other end of the column is assumed to be at the origin. The probability that a given column will be terminated in the distance $d\ell$ is $\alpha(\ell)d\ell$, so we have the relations between $P(\ell)$ and $\alpha(\ell)$:

$$P(\ell) = P(\ell - d\ell) \cdot [1-\alpha(\ell) \cdot d\ell], \qquad 1)$$

$$dP = -P(\ell) \cdot \alpha(\ell) \cdot d\ell. \qquad 2)$$

The probability, $g(\ell) \cdot d\ell$, of finding a column with a length between ℓ and $\ell+d\ell$ will be $P(\ell)$ times $\alpha(\ell) \cdot d\ell$. Equation 2 has a simple exponential solution for $P(\ell)$ when $\alpha(\ell)$ is a constant, so the

probability distribution for column lengths is:

$$g(\ell) = \frac{1}{\langle \ell \rangle} \cdot \exp\left(\frac{-\ell}{\langle \ell \rangle}\right). \qquad 3)$$

The Fourier transformation of Eqn. 3 gives a Lorentzian function for the XRD peak shapes. The boundaries and regions of high dislocation density that we have identified in TEM micrographs (see below) show many different separations, but we have not observed enough of them to compile statistics on their distributions. Perhaps the best justification that $\alpha(\ell)$ is a constant (equal to $\langle \ell \rangle^{-1}$) is that XRD peaks from overtempered and cold-worked material have a Lorentzian-like profile. This approach predicts that the full-width-at-half-maximum (FWHM) of the Lorentzian components, when linearized in k-space by multiplying by the factor $\cos\theta$, should be independent of the order of reflection. In fact, the corrected widths of the Lorentzian components of the martensite peaks did not increase significantly with the modulus of the diffraction vector. The Lorentzian component widths of the austenite peaks, however, did show a partial tendency to scale with the modulus of the diffraction vector.

Nevertheless, the assumption that $\alpha(\ell)$ is independent of ℓ requires further discussion. When the dislocations are tightly formed into cell walls of random separation, the Khachaturyan approach applies for most of the material in the cell interiors. Wilkens [47] has approached the problem of x-ray line broadening in plastically deformed material with a direct theoretical treatment of elastic strain fields around dislocations. The range of elastic distortions from dislocations in the cell walls is small, and the size distribution of the cell interiors will produce a Lorentzian diffraction profile with its broad tails. Additional intensity in the tail region will arise from x-ray diffraction by the material in the cell walls. However, when the dislocations are more homogeneously distributed throughout the material their elastic distortions extend over a longer range, and $\alpha(\ell)$ tends to become linear in ℓ. The shape of the diffraction profile tends towards a Gaussian function [47,48]. Our association of Lorentzian components of the XRD profile with dislocation distributions is therefore less appropriate when the dislocations are more homogenously distributed throughout the material.

Analysis of XRD Peak Shapes

The width of the strain distribution, $\Delta\varepsilon$ was determined from the FWHM of the Gaussian component of the Rachinger and Stokes corrected peak shape, $G(\theta)$, with θ in radians, by using the relationship:

$$\Delta\varepsilon(\theta) = \cot(\theta) \cdot G(\theta) \; . \qquad 4)$$

The widths of the strain distributions in the austenite and the martensite are shown in Fig. 21 as a function of tempering time. The $(220)\gamma$ and $(311)\gamma$ peaks, and the $(200)\alpha'$ and $(211)\alpha'$ peaks had measured strain distributions that differed by about 20% in width, but this was considered to be experimentally insignificant and these data were averaged for presentation in Fig. 21. Some systematic errors of

10-20% in strain distribution are expected from our method of data processing. Nevertheless, our strain distribution data for martensite seems roughly consistent with data from a HSLA steel that were obtained by the method of multiple orders [49]. For all materials the strain distribution in the austenite was about twice as large as the strain distribution in the martensite (see Fig. 21). The strains in both the austenite and the martensite remain essentially constant with further tempering. Cold rolling had no effect on the widths of the strain distributions. Immersion in liquid nitrogen had a small, and perhaps insignificant, effect on only the overtempered material. Error bars are drawn to indicate our overall confidence in the data of Figs. 21 and 22. Our confidence in the trends in particle size data (Fig. 22) is greater than our confidence in the trends in strain distribution data (Fig. 21) because the changes in peak broadening due to size effects were larger.

The average sizes of the diffracting domains were determined from the Scherrer approximation for a column of coherently diffracting planes of length ℓ [29]:

$$\ell = \frac{\lambda}{L(2\theta)\cdot\cos(\theta)} \quad . \qquad 5)$$

Here $L(2\theta)$ is the FWHM of the Lorentzian component of the diffraction peak in radians, and λ is the x-ray wavelength. The average sizes of diffracting domains of the austenite and martensite are shown as a function of tempering time in Fig. 22. The austenite sizes are presented as an average of data from the $(220)\gamma$ and $(311)\gamma$ peaks, which showed very similar behavior. The average martensite sizes extracted from the $(200)\alpha'$ peaks were about 20% smaller than the sizes obtained from the $(211)\alpha'$ peak, but their average is presented in Fig. 22. The increase in size that is shown for the austenite over the first ten hours of tempering is consistent with the growth in size of the austensite particles seen in TEM micrographs. With further tempering, however, the mean sizes of x-ray diffracting domains are reduced, and this does not correspond to decreased dimensions of austenite particles or martensite laths observed with TEM.

Dislocation Structures

The average sizes of diffracting domains of both the austenite and the martensite are perhaps reduced slightly between 10 and 100 hrs of tempering, but large domains produce only slight line broadenings that are difficult to measure accurately. However, the abrupt reduction in mean size of diffracting domains that occurs after 100 hrs of tempering is unmistakable (see Fig. 22). Immersion in liquid nitrogen had no effect on the average size of the austenite or martensite of material tempered less than 100 hrs. However, liquid nitrogen immersion resulted in a 20% reduction in austenite size for material tempered for more than 100 hrs. Liquid nitrogen immersion also caused a 5-10% reduction in martensite size for the material tempered for 750 hrs, but the reduction in martensite size for material tempered for 240 hrs was very small. A similar reduction in average size of the martensite and austenite was always produced by cold rolling at room temperature.

In material that was not cold rolled, the reductions in size of the austenite and the martensite diffracting domains correlated with the transformation of some of the austenite. Qualitatively, the greater the extent of the transformation, the greater the reduction in size of coherently diffracting domains. We first tried to explain these large reductions by assuming a small effective size for only the fresh martensite and the tempered martensite immediately around it. This seemed reasonable because TEM showed that these regions of martensite have a very defective crystal structure. Accordingly, we tried to fit these broadened martensite diffraction profiles to a sum of two functions. The first function was attributed to the tempered martensite and had a narrow lineshape comparable to that of Fig. 1a. The second function, which had 10-15% of the integrated intensity of the first, was attributed to the defective martensite and had a broad Lorentzian lineshape of adjustable width. The quality of fit to the experimental peaks was clearly worse than the fit to a single convolution of a Gaussian and a Lorentzian function. We conclude that the large reduction in average size of the martensite diffraction domains reflects bulk changes in the tempered martensite, and not just the defect structure of a small amount of the martensite.

The large reduction in average size of the martensite diffraction domains is due to the dislocation structures that radiate outwards from the fresh martensite and across the tempered martensite (see Figs. 9, 13 and 14). The average size of martensite diffraction domains for material tempered for 240 hrs is 530 A. This is comparable to the separation between the rough lines in Figs. 9 and 13, so these rough lines are identified as those dislocation cell walls that destroy the coherence of x-ray diffraction between adjacent blocks of tempered martensite. The more diffuse dislocation distribution seen in Fig. 14 would also be responsible for such a reduction in the mean size of diffraction domains, but the complexity of this dislocation distribution impairs the quantitative analysis of XRD peak broadenings.

Very much like for martensite, XRD data for austenite show a significant reduction in the average size of diffraction domains after cold rolling or overtempering (see Fig. 22). We believe that the formation of dislocation structures in the austenite is at least partially responsible for this reduction. The TEM images of the remaining austenite in Fig. 14 may show some defect structure. In addition, the background contrast in the TEM image of the austenite in Fig. 13 changes between its left and right sides, suggesting a region of crystallographic disregistry in the center of the particle.

In a recent experimental study of deformed copper single crystals by Ungar, et al. [50], broadenings of (200)Cu peaks were successfully separated into a component due to highly dislocated material in the dislocation cell walls, and a component due to material in the cell interiors. Although such a dislocation cell structure is evident in the TEM micrographs of Figs. 9 and 13, a two-component decomposition of our (211)α' diffraction profiles from overtempered material cannot improve the quality of fit in an experimentally significant way. In general the resolution of our data does not justify this decomposition, especially since the two components are expected to be of comparable widths and of

significantly different intensities [50]. For cold-rolled material, however, the (211)α′ diffraction peak of Fig. 1c shows an asymmetry that suggests a two-component decomposition. This asymmetry from (211)α′ planes parallel to the plane of rolling is qualitatively consistent with the Poisson contraction of the material in the dislocation walls, as suggested by Ungar, et al. for copper tensile specimens [50]. (Our rolling direction was perpendicular to the diffraction vector.) Evidently this asymmetry does not arise because the fresh martensite has a smaller lattice parameter than the tempered martensite; the broad (211) α′ peaks from overtempered but unrolled material (Fig. 1c) are symmetric.

Mechanical Properties

The temperature dependence of the Charpy impact energy for materials with each tempering time are shown in Fig. 3. The approximately 130 data points are not individually shown on Fig. 3, but their standard deviations were about 7 J. These data show a general agreement with data from Kim and Schwartz [11]. However, our material exhibits a higher upper shelf toughness and a lower DBTT. None of these curves show a complete transition to a brittle "lower shelf toughness"; the Charpy energy appears to be still decreasing at 77 K. Testing Charpy specimens at temperatures below 77 K is both difficult and uninformative. The low heat capacity of metals at these temperatures allows the heat generated during deformation to produce large increases in temperature in front of the crack tip (>50 K) [51]. So without a lower shelf toughness for comparison, we choose a uniform criterion for all materials by defining the DBTT as the temperature at which the Charpy energy falls to 120 J. With linear extrapolation for some of the curves in Fig. 3, the DBTT depends on tempering time as shown in Fig. 4. Some Charpy specimens were broken at room temperature after four cycles of liquid nitrogen immersion. These data are represented by points at 290 K in Fig. 3.

III. DISCUSSION

We first discuss the quality of the austenite/martensite interface, and suggest that the crystallographic orientation relation between the austenite and martensite results from how the austenite nucleates at the surfaces of the martensite laths. However, our primary effort is directed towards understanding the stability of precipitated austenite and the microstructural consequences of its transformation. Finally, we speculate on mechanical effects associated with the transformation of the austenite.

We seek mechanisms which reduce the austenite stability with tempering time. In the first 100 hrs of tempering the microstructure changes gradually, the main changes noted so far being the growth of the

---

* Which were 0.2% C from austenite lattice parameter and 0.3% C from martensite lattice parameter plus volume fraction of austenite.

austenite particles and their eventual reduction in carbon concentration. The reduction in the M_s temperature of precipitated austenite is expected to be ~500° for each additional 1% reduction in carbon concentration. Therefore our reductions in austenite carbon concentrations* during the first 81 hrs of tempering are too small to fully account for the observed loss of austenite stability during tempering. Furthermore, the increasing nickel concentration of the austenite during tempering [25] is a source of austenite stability that must also be overcome.

We have observed two other microstructural changes that occur as the austenite becomes unstable. The first is the reduced coherency of the austenite/martensite interface. The energetics of this coherency loss are probably small, but the nucleation of the martensitic transformation of the austenite could be related to the quality of the austenite/martensite interface. The second microstructural change is the two types of dislocation structures that are formed around the transforming austenite particle. The energies associated with the formation of these dislocation structures are large enough to affect the thermodynamics of the transformation. These defect structures have many similarities to the defect structures produced by cold work, and we suggest that the mechanical effects of the transformation are due in part to this defect structure.

Austenite Stability and Austenite/Martensite Interface Coherency

The Kurdjumov-Sachs orientation relationship minimizes the energy associated with the orientation of an austenite crystal with respect to the orientation of the martensite. The energetics of atomic fit at the austenite/martensite interface are responsible for this orientation energy as well as for some features of the austenite/martensite interface. The new austenite is coherent over small areas of interface (~100 A linear dimension). Interface dislocations lie between these coherent areas. The high quality of atomic fit at the interface is so energetically favorable that it offsets the energy of formation of the interface dislocations. This tendency for the atoms in the austenite to be favorably arranged over as much of the austenite/martensite interface as possible may also be the reason why an austenite particle tends to form the same Kurdjumov-Sachs variant during multiple thermal cycles [4].

Interface dislocations are required at the austenite/martensite interface when it is formed at 600°C because the mismatch between $(111)\gamma$ and $(110)\alpha'$ planes is more than 2%. Because the austenite forms slowly at temperatures when all atoms are mobile, there will be no long-range stresses across the austenite/martensite interface at 600°C. As the austenite forms, the transformation strains are accommodated by a macroscopic contraction of the material; this is the contraction that was previously measured by high temperature dilatometry [38]. However, after cooling to room temperature the thermal contraction differences between the austenite and the martensite should leave the austenite in a

state of tension*. At room temperature the atoms are not sufficiently mobile to relax this tension. The presence of these strains due to thermal contraction is suggested by the dark strain contrast loops seen around the austenite particles in Fig. 14. The small compositional and morphological changes of the austenite during tempering suggest that the strains due to thermal contraction will change only slightly with tempering time.

The observed correlation between the loss of austenite/martensite interface coherency and the loss of austenite stability in cold-rolled and overtempered material suggests a causal relationship between austenite stability and interface coherency. This correlation alone cannot show which phenomenon is the cause and which is the consequence. The loss of interface integrity precedes the transformation of an austenite particle. Possibly the loss of coherency at the austenite/martensite interface facilitates the nucleation of the transformation. The austenite stability would then be reduced with tempering time because the interface coherency is reduced with tempering time. On the other hand, it is also possible that the transformation of some of the precipitated austenite is responsible for the loss of coherency at other surviving austenite/martensite interfaces. This could occur by the movement of dislocations from the transforming particle to other austenite/martensite interfaces, which may act as sinks for dislocations because they are under stresses from differential thermal contractions. This process is suggested by Fig. 14a, in which the small untransformed austenite particle towards the bottom left corner of the figure is engulfed by dislocations sent from the large transformed particles on its sides. These two possibilities are not mutually exclusive. An autocatalytic chain reaction can be envisioned in which the transformation sends off dislocations that reach a second austenite/martensite interface. The resultant loss of interface coherency could encourage the transformation of this second austenite particle, which could then send more dislocations to other interfaces.

Transformation of Precipitated Austenite

Transformation Strains

Speaking metaphorically, the transformation of an austenite particle is a small explosion detonated within the tempered martensite. To estimate the transformation strains, we note that the volume per atom in the austenite in materials with some fresh martensite is about 3.5% less than that of the surrounding martensite. This is probably close to the actual volume dilatation of the transformation because corrections due

---

* Our present dilatometry work showed that the difference between the amount of unrestrained thermal uxpansion of the austenite and the martensite is more than 0.5% in length. This strain is greater than the elastic limit in a tensile test, but it is a stress-free strain, so for austenite particles constrained by martensite the thermal contraction may not necessarily be large enough to cause plastic deformation upon cooling.

to the facts that the austenite is under tension, but contains most of the carbon are approximately cancelling. Only a little microtwinning is observed in the fresh martensite particles. Microtwinning permits some cancellation of the shear components of the transformation strains, so its absence suggests that shear strains around the fresh martensite particles will be large.

Due to these large strains, the transforming austenite particles are potent generators of dislocations. When some austenite particles had transformed, we observed dislocations that extended well into the tempered martensite (and tended to form into cell walls), and a second type of structure best described as a dense mesh of dislocations around the transformed particles. These dislocations were sometimes mobile under electron beam heating, suggesting that large stresses still remain in the material around the transformed particles. Defects in the bulk austenite around fresh martensite particles were previously reported by Krauss [53], and they were also interpreted as plastic accommodation of the transformation strains. The elastic and plastic strains inside the transformed particle are probably so severe that the particles always appear dark in bright field micrographs.

Figure 18 shows that when some of the austenite transforms, part of the transformation strain is accommodated by the remaining austenite, leaving it with a net hydrostatic compression. At the same time, the martensite is not strongly compressed. The strong compression of the remaining austenite probably arises because some individual austenite particles do not undergo a complete transformation. The partial transformation of an austenite particle is seen in Figs. 9 and 14, and in previous work [19,53]. Because of their proximity, the untransformed parts of the particle must accommodate much of the transformation strain. The austenite is in a state of tension before some of it transforms, after which the remaining austenite is in a state of compression. (This is consistent with our measurement of 3.582 A for the lattice parameter of an annealed austenitic Fe-31%Ni alloy, which is smaller than the tensioned lattice parameter of the austenite in material tempered for less than 100 hrs but larger than the compressed lattice parameter of overtempered or cold-rolled material.)

Next, we argue that the energy required to form the dislocation structures around the transforming particles affects the thermodynamics of the transformation of the precipitated austenite and can reduce the stability of the austenite particles as they grow larger during tempering. The movement of these dislocations helps to relieve the local elastic stresses that would otherwise impede the transformation. It is interesting to point out that the elastic stresses that accompany the transformation probably do not affect the stability of the austenite particles as they grow larger. Since the transformation strains are so large, they must be primarily accommodated by plastic strains. Only a small fraction of the transformation strain energy remains as elastic energy. Furthermore, the residual elastic energy should tend to scale with the volume of the transformed particle. Therefore the small elastic energy barrier per volume of transformation will not change with tempering time. On the other hand, we now show that large changes in

plastic strains around transformed particles can affect the free energy of the transformation.

Two Types of Dislocation Structures and Their Energies

We have observed a dense dislocation structure around the surfaces of fresh martensite particles of many different sizes. That much of the plastic accommodation occurs near the fresh martensite/tempered martensite interface is reasonable because the stresses will be largest close to the transforming particle, and the interface has already been weakened by interface dislocations. Presumably the dislocations remain near the interface because they tangle soon after they are formed. The amount of dislocation activity, i.e., the increase in the number of useful dislocations times their Burgers vector and mean free path, needed to accommodate the transformation of an austenite pasticle scales with the volume of the particle. We suggest that the surface dislocation structure would not be so effective in accommodating the transformation of large particles because the number of dislocations in it times the length they have moved probably scales with the surface area of the particle.

Instead, when there is a transformation of austenite particles larger than about 0.5 μm, it appears that more slip occurs in the tempered martensite away from the transforming particle. This slip involves a longer mean free path for each generated dislocation. A given amount of strain therefore requires fewer dislocations and a lower total energy expenditure for their formation. If we assume that this formation energy is an important part of the energy required for plastic deformation, then as the austenite particles grow larger, the specific energy required to accommodate the transformation strains is reduced.

We can estimate thermodynamic effects on the transformation that arise from a change in the type of transformation-induced dislocation structures. A high energy of formation is associated with the dense surface dislocation entanglements around transformed particles. Assuming a dislocation density of $10^{13}/cm^2$ and an energy of 2 eV per atomic length of dislocation line, then if these entanglements occupy 10% of the bulk material when 10% of the material has freshly transformed to martensite, an energy of 0.01 eV/atom must be subtracted from the free energy difference that drives the transformation of the austenite particles. If we follow the Clausius-Clapeyron derivation for the equilibrium temperature of two phases [54], we expect a shift in the M_D temperature, ΔT, of:

$$\Delta T = \frac{-(0.01\ eV) \cdot M_D}{L} \qquad 7)$$

Using a value for the latent heat, L, of 0.02 eV/atom [55-58], we find a change in M_D of at least -150 K associated with the formation of the surface dislocation structure around the transformed particles.

We have already suggested that the other type of more extended dislocation structure in the tempered martensite requires less formation

energy to accommodate a given transformed volume. When the transformation is accommodated with this more extended dislocation structure, M_D will not be so strongly suppressed. It seems plausible that the changes in defect structures around larger transforming particles can cause M_D to increase by more than 100 K. In essence, the austenite stability is reduced as the particles grow larger because the accommodation of the transformation strains apparently requires less energy.

Additionally, for the dense dislocation entanglements around the transformed particles some of the formation energy probably scales with the surface area of the particle. Hence, these defect structures probably provide a surface energy barrier to the transformation that is most significant for small particles with large surface/volume ratios. As the austenite particles grow larger this surface energy barrier becomes less important, so the austenite particles will lose stability with increased tempering time.

Effects of Tempering on Mechanical Properties

Early Stages of Tempering

We did not compare untempered material with tempered material, but the suppression of the ductile-to-brittle transition temperature (DBTT) in 9Ni steel after a short tempering is well known. It appears from Figs. 3 and 4 that the lowest DBTT is achieved after several hours of tempering. Although the hardness decreases rapidly during the first few minutes of tempering [11,59], on the time scale of a few hours there is a small reduction in hardness (see Fig. 5) and a small reduction in upper shelf toughness (see Fig. 3). Using data for martensitic steels [60,61], the observed hardness decrease of 1 unit corresponds to a carbon concentration reduction of 0.04% in the martensite. This seems consistent with the changes in martensite carbon concentration deduced from x-ray lattice parameters, so the early changes in mechanical properties could be due to carbon segregation to the austenite. Additionally in these first few hours, more precipitated austenite has formed and the martensite defect structure has recovered; these changes could also contribute to the early changes in mechanical properties.

Although the changes in mechanical properties after several hours of tempering were not consistent with the role of austenite as a scavenger, the scavenging of interstitial elements by the austenite in the early stages of tempering (within 3 hrs for our material) may affect mechanical properties, especially at the higher temperatures. The data of Fig. 3 differ from corresponding data of Kim and Schwartz [11], which show a large improvement in toughness between 0.16 and 10 hrs of tempering at 595°C. This difference in Charpy toughness may be due to the higher concentration of sulfur in their material (0.01% vs. our 0.004%) and a difference in their heat treatment (their as-received plate was Q-treated directly). Perhaps the dissolution of inclusions that are detrimental to upper shelf toughness was occurring during the tempering of their material. Indeed, Kim and Schwartz conclude that the principal role of the austenite was to serve as a sink for deleterious elements, and this sink worked better when more austenite was present. However,

they also reported a deterioration in Charpy toughness after 10 hrs of tempering.

Austenite Stability and Charpy Toughness

Over a wide range of tempering times, the Charpy toughness correlates better with the stability of the austenite than with the total amount of austenite in the material. In particular, after tempering at 590°C for 10 hrs, the toughness of 9Ni steel at temperatures below 200 K begins to deteriorate, even though the amount of austenite continues to increase. This deterioration proceeds gradually up to 100 hrs of tempering, but after 100 hrs of tempering the austenite has become quite unstable, and the cryogenic toughness deteriorates sharply. Evidence that the austenite stability influences low temperature brittle fracture behavior is provided by a comparison of the systematics of Fig. 6 with Fig. 4; as the austenite loses stability with tempering time the DBTT of the material increases.

No precipitated austenite is completely stable against large mechanical deformations at low temperatures; previous work with 9Ni steel and 6Ni steel [3,11,18,19] has shown that all of the precipitated austenite has transformed to martensite in the very highly strained region near the fracture surface. So even for materials with very stable retained austenite and excellent cryogenic toughness, at least some of the austenite transforms completely to martensite during the fracture process. We suggest that the mechanical consequences of the transformation of austenite particles during a toughness test will depend on when the transformation occurs. Specifically, the transformation of the austenite will have different effects on the Charpy toughness if it occurs close to or far from the crack tip. Since the stability of the austenite particles determines when their transformation occurs, a correlation between austenite stability and Charpy toughness is expected.

One reason for the correlation between austenite stability and Charpy toughness could be that the transformation away from the crack tip is detrimental to toughness. We have observed the microstructural changes in the vicinity of the transformed particles in overtempered materials having unstable austenite and low toughness. These microstructural changes show many similarities to the changes caused by cold-work (a sharp reduction in austenite lattice parameter, a reduction in mean size of the austenite and martensite diffracting domains and qualitatively similar dislocation structures seen in TEM). Since cold work is detrimental to cryogenic Charpy toughness, we expect the local work-hardening around the transformed particles to increase the hardness, reduce the ductility, and facilitate crack propagation in the material*. We therefore suggest that low temperature brittle behavior is promoted

---

* Figs. 3 and 5 show that the hardness of the overtempered material is increased and its toughness is decreased after an immersion in liquid nitrogen transforms much of the austenite. (However, the hardness of the fresh martensite is also expected to contribute to this hardness increase.)

by the microstructural damage around the transformed particles. In other words, the transformation of precipitated austenite is detrimental to toughness if the austenite transforms too easily. The data of Figs. 4 and 6 show that as the austenite transforms more easily, there is an increase in the DBTT. This supports the idea that the transformation of austenite away from the crack tip is detrimental but, since the stability of the austenite is decreasing, there is also less austenite present to transform near the crack tip.

A second reason for the correlation between the austenite stability and Charpy toughness could be that the transformation very close to the crack tip is beneficial to toughness. We have not observed the microstructure in material close to the crack tip for materials with both stable and unstable austenite*. However, it is conceivable that the dislocation structures will be qualitatively different depending on whether or not the austenite particle transformed near the crack tip. For very stable austenite particles the applied stress in which the particles transform is comparable to the stresses developed by the transformation itself (somewhat more than the yield stress). Because such large applied stresses are required in order to transform the stable austenite particles, the dislocations that are generated will move into the tempered martensite in response to the applied stress as well as the transformation stress. By LeChatelier's principle the dislocations should move so as to reduce** the applied stress. By reducing the stress intensity within a packet of laths, the mean length of cleavage planes should be reduced and, therefore, the DBTT should be suppressed.

Comparison with Other Models

Models have been proposed to explain how the transformation of an austenite particle can relieve the stress intensity near a transforming particle. A model by Antolovich, et al. [23] relies on the shape change of the transforming particle to provide the local stress relaxation. Although such mechanisms may be important for materials with large amounts of transforming austenite, it was recognized by Kim and Schwartz [11] that the transformation of the small amounts of austenite in 9Ni steel will be mechanically ineffectual. Our hypothesized interaction between the applied stress and the dislocation structures generated by the transformation will predict similar experimental systematics to the shape change models, but it does not rely on the small energies associated with the stress times that shape change. Unfortunately, it is

---

* The dislocation structure around particles that transformed near a crack tip is seen in Ref. [3], and these dislocation structures may tend to orient along lath axes rather than merely radiating from austenite particles.

** This same argument can be made more mechanistic by using the linearity of the Peach-Koehler equation for the force on a dislocation line [62]. The total force will be the sum of the force due to the applied stress and the force due to the transformation strains.

difficult to quantify the amount of stress relaxation caused by our proposed mechanism.

In the model proposed by Morris, et al. [21,22], which can also account for the correlation between the austenite stability and the cryogenic fracture toughness, the thermal transformation of the austenite has a neutral effect on mechanical properties. By transforming to the same crystallographic variant of martensite as its neighboring laths, the unstable austenite particle will not affect the brittle cooperative cleavage of packets of laths. In the dislocation accommodation model proposed here, the transformation of an unstable austenite particle is detrimental to fracture toughness because it introduces uncontrolled cold work into the material. Both models attribute beneficial effects to the transformation of stable austenite in a large applied stress. However, in the model of Morris, et al. the role of the applied stress is to force a particular crystallographic variant of the fresh martensite particle. Because this variant differs from that of its neighboring laths, the fresh martensite impedes the brittle cooperative cleavage of packets of laths. In the dislocation accommodation model proposed here, the applied stress intensity is fundamentally important because it helps to direct the motion of those dislocations that are formed during the transformation. Devising an experiment to evaluate the relative mechanical significance of these two models will be difficult because they predict many similar experimental systematics. Evidence favoring one model or the other must come from detailed observations of fresh martensite particles that transformed near the crack tip.

IV. SUMMARY AND CONCLUSIONS

During the first few hours of tempering at 590°C, the austenite that forms in 9Ni steel is thermally stable and reasonably mechanically stable. This austenite is small and atomically coherent with the surrounding martensite laths over ~100 A distances. The high quality of this interface suggests that the energetics of atomic matching at the austenite/martensite interface are responsible for the Kurdjumov-Sachs orientation of the precipitated austenite with respect to the surrounding martensite laths. This interface remains undisturbed at low temperatures, and differential thermal contraction leaves the austenite in a state of tension at room temperature. The austenite initially maintains a constant carbon concentration of somewhat more than 0.5% as it grows, so it serves as a sink for carbon. A recovery of the defect structure in the martensite also occurs during the first few hours of tempering. After about 10 hrs of tempering, the carbon content of the martensite has been reduced to its near-zero solubility limit, and the austenite particles are not supplied with any more carbon as they become larger. The carbon concentration of the austenite is reduced and the austenite loses stability with further tempering. However, the reduction in austenite carbon concentration is not large enough to fully account for the loss of austenite stability during tempering.

In material tempered for about 100 hrs, the austenite/martensite interface has begun to lose coherency, and some austenite particles have

begun to transform. Although the nucleation of the transformation of austenite particles could be promoted by the loss of interface coherency, we believe it equally possible that the loss of interface coherency is a consequence of the transformation of other austenite particles. Much of the accommodation of the large transformation strains occurs by local plastic deformation in all components of the microstructure. The transforming particles serve as potent generators of dislocations in the tempered martensite. Some accommodation of the transformation strains is provided by a dense dislocation entanglement in the tempered martensite near the transformed particles. Other dislocations extend deeply into the tempered martensite, and tend to form into dislocation walls. It appears that the dislocation structures around transformed particles in overtempered material are more extended, and therefore fewer dislocations are required for a given amount of plastic accommodation. The energy barrier per unit volume of transformation may therefore be lower when large particles transform. In addition, we suggest that the loss of stability of the austenite as it grows could also be due to a scaling of some energy in the dislocation structure with the surface/volume ratio of the austenite particles.

The dislocation structures around thermally transformed austenite particles are microscopically similar to the defect structures induced by cold work. We therefore expect that the formation of a thermally unstable or weakly mechanically stable precipitated austenite is deleterious to cryogenic Charpy toughness. On the other hand, a more mechanically stable austenite particle will transform closer to the crack tip. It is suggested that the defect structures created during the transformation of austenite may be qualitatively different when the transformation occurs in material subjected to a high stress.

ACKNOWLEDGMENTS

This work was supported by the Director, Office of Basic Energy Science, Materials Science Division of the U. S. Department of Energy under contract no. DE-AC03-76SF00098.

REFERENCES

1. G.R. Brophy and A.J. Miller: Trans. ASM, 1949, vol. 41, p. 1185.

2. A.W. Pense and R.D. Stout: Weld. Res. Council Bull. 205, 1975.

3. C.K. Syn, B. Fultz and J.W. Morris, Jr.: Met. Trans. 1978, vol. 9, p. 1735.

4. C.K. Syn, S. Jin and J.W. Morris, Jr.: Met. Trans. A 1977, vol. 7, p. 1827.

5. S.K. Hwang, S. Jin and J.W. Morris, Jr.: Met. Trans. A, 1975, vol. 6, p. 2015.

6. J.I. Kim and J.W. Morris, Jr.: Met. Trans. A 1981, vol. 13, p. 1957.

7. C.W. Marschall, R.F. Heheman and A.R. Troriano: Trans. ASM, 1972, vol. 55, p. 135.

8. T. Ooka and K. Sugino: J. Japan Inst. Metals, 1976, vol. 30, p. 435.

9. T. Ooka, H. Mimura, S. Yano, K. Sugino and T. Toizumi: J. Japan Inst. Metals, 1976, vol. 30, p. 442.

10. H. Sakurai, S. Yano, T. Inoue, H. Mimura and K. Aoki: J. Japan Inst. Metals, 1969, vol. 33, p. 857.

11. K.J. Kim and L.H. Schwartz: Mater. Sci. Eng., 1978, vol. 33, p. 5.

12. T. Funekoshi: Ph.D. Thesis, Tohuku Univ., Japan, 1973.

13. S. Nagashima, T. Ooka, S. Sekino, H. Mimura, T. Fujishima, S. Yano and H. Sakurai: Trans. Iron Steel Inst. Japan, 1971, vol. 2, p.402.

14. J.R. Strife and D.E. Passoja: Met. Trans. A, 1980, vol. 11, p. 1341.

15. M. Kron, A. Constant, A. Clerc, J. Plateau, G. Henry, M. Robert and C. Crussard: Memoires Scientifiques Rev. Metallurg., 1971, vol. 58, p. 901.

16. D. Hardwick: Iron Steel, 1971, vol. 34, p. 414.

17. H. Haga: Trans. Iron Steel Inst. Japan, 1973, vol. 13, p. 141.

18. B. Fultz: M.Sc. Thesis, Univ. of California, Berkeley, 1978.

19. B. Fultz and J.W. Morris, Jr.: Met. Trans. A, in press.

20. J.I. Kim: Ph.D. Thesis, Univ. of California, Berkeley, 1979.

21. J.W. Morris, Jr., C.K. Syn, J.I. Kim and B. Fultz: Proc. Inter.-Conf. Martensitic Transform., 1979, MIT Cambridge, Mass., p. 573.

22. J.I. Kim, C.K. Syn and J.W. Morris, Jr.: Met. Trans. A, 1983, vol. 14, p. 93.

23. S.D. Antolovich, A. Saxena and G.R. Chanani: Met. Trans. A, 1974, vol. 5, p. 623.

24. B. Fultz: Ph.D. Thesis, Univ. of California, Berkeley, 1982.

25. B. Fultz, J.I. Kim and J.W. Morris, Jr.: to be published.

26. Annual Book of ASTM Standards, E-23 "Notched Bar Impact Testing of Metallic Materials", and A-370 "Mechanical Testing of Steel Products", (1980), ASTM, Philadelphia.

27. R.L. Miller: Trans. ASM, 1964, vol. 57, p. 893. R.L. Miller: Trans. ASM, 1968, vol. 61, p. 593.

28. B.E. Warren and B.L. Averbach: J. Appl. Phys., 1950, vol. 21, p. 595.

29. B.E. Warren: X-Ray Diffraction, Chap. 13, Addison-Wesley, Reading, Mass., 1969.

30. B.E. Warren: Prog. Metal Phys., vol. 8, B. Chalmers and R. King, eds., 1959, Pergamon Press, New York, p. 159.

31. W.A. Rachinger: J. Sci. Instr., 1948, vol. 25, p. 254.

32. A.R. Stokes: Proc. Phys. Soc. London, 1948, vol. 61, p. 382.

33. B. Fultz and J.W. Morris, Jr.: Rev. Sci. Instr., 1978, vol. 49, p. 1216.

34. B. Fultz: Radiation Detector, 1983, U. S. Patent # 4,393,307.

35. B. Fultz and J.W. Morris, Jr: Nucl. Instr. Methods, 1981, vol. 188, p. 197. B. Fultz and J.W. Morris, Jr.: Nucl. Instr. Methods, 1983, vol. 211, p. 569.

36. S. Margulies and J.R. Ehrman: Nucl. Instr. Methods, 1971, vol. 1:, p. 131. S. Margulies, P. Debrunner and H. Frauenfelder: Nucl. Instr. Methods, 1973, vol. 21, p. 217.

37. G. Kurdjumov and G. Sachs: Z. Physik, 1930, vol. 64, p. 335.

38. J.I. Kim and J.W. Morris, Jr.: Met. Trans. A, 1980, vol. 11, p. 1401.

39. W.B. Pearson: A Handbook of Lattice Spacings and Structures of Metals and Alloys, Pergamon Press, New York, 1958.

40. A.D. Romig, Jr. and J.I. Goldstein: Met. Trans. A, 1978, vol. 9, p. 1599.

41. N. Ridley, H. Stuart and L. Zwell: Trans. AIME, 1979, vol. 245, p. 1834.

43. Z. Nishiyama as referenced by Pearson, ibid, and Sci. Rep. Tohoku Imp. Univ., 1935, vol. 24, p. 128.

43. B.P.J. Sandvik and C.M. Wayman: Met. Trans. A, 1983, vol. 14, p. 833.

44. B.Y. Pines and A.F. Sirenko: Sov. Phys. Cryst., 1963, vol. 7, p. 15.

45. R.L. Rothman and J.B. Cohen: Advances in X-Ray Analysis, 1979, vol 12, C.S. Barrett, J.B. Newkirk and G.R. Mallett, eds., Plenum Press, New York, p. 208.

46. A.G. Khachaturyan: Sov. Phys. Cryst., 1960, vol. 5, p. 335.

47. M. Wilkens: Phys. Stat. Solidi, 1970, vol. 2, p. 359.

48. M.A. Krivoglaz and K.P. Ryaboshapka: Fiz. Metal. Metalloved., 1963, vol. 15, p. 18.

49. S.I. Kwun and R.A. Fournelle: Met. Trans. A, 1980, vol. 11, p. 1429.

50. T. Ungar, H. Mughrabi, D. Ronnpagel and M. Wilkens: Acta Metall., 1984, vol. 32, p. 333.

51. W.G. Dobson and D.L. Johnson: Adv. Cryogenic Eng. Materials, vol. 30, R.P. Reed and A.F. Clark, eds., Plenum Press, New York, in press.

52. G. Krauss, Jr,: Acta Met., 1973, vol. 11, p. 499.

53. Y.H. Kim: unpublished results, Univ. of Calif., Berkeley, 1983.

54. C. Kittel: Thermal Physics, 1969, John Wiley, New York, p. 327.

55. L. Kaufman and M. Cohen: Prog. Metal Phys., 1958, vol. 7, B. Chalmers and R. King, eds., Pergamon Press, New York, p. 165.

57. M.A. Krivoglaz and V.D. Sadovskiy: Fiz. Metal. Metalloved., 1964, vol. 18, p. 23.

57. L.V. Voronchikhin and I.G. Fakidov: Fiz. Metal. Metalloved., 1976, vol. 21, p. 119.

58. E.I. Estrin: Fiz. Metal. Metalloved., 1975, vol. 19, p. 119.

59. H.J. Kim and H. Shin: unpublished results, Univ. of Calif., Berkeley, 1982.

60. Metals Handbook, 9th ed., 1978, vol. 1, ASM, Metals Park, OH, pp. 458, 472, 530.

61. Glossary of Metallurgical Terms and Engineering Tables, 1979, ASM, Metals Park, Ohio, p. 89.

62. M.O. Peach and J.S. Koehler: Phys. Rev., 1950, vol. 80, p. 437. J.P. Hirth and J. Lothe: Theory of Dislocations, McGraw-Hill, New York, 1968, p. 102.

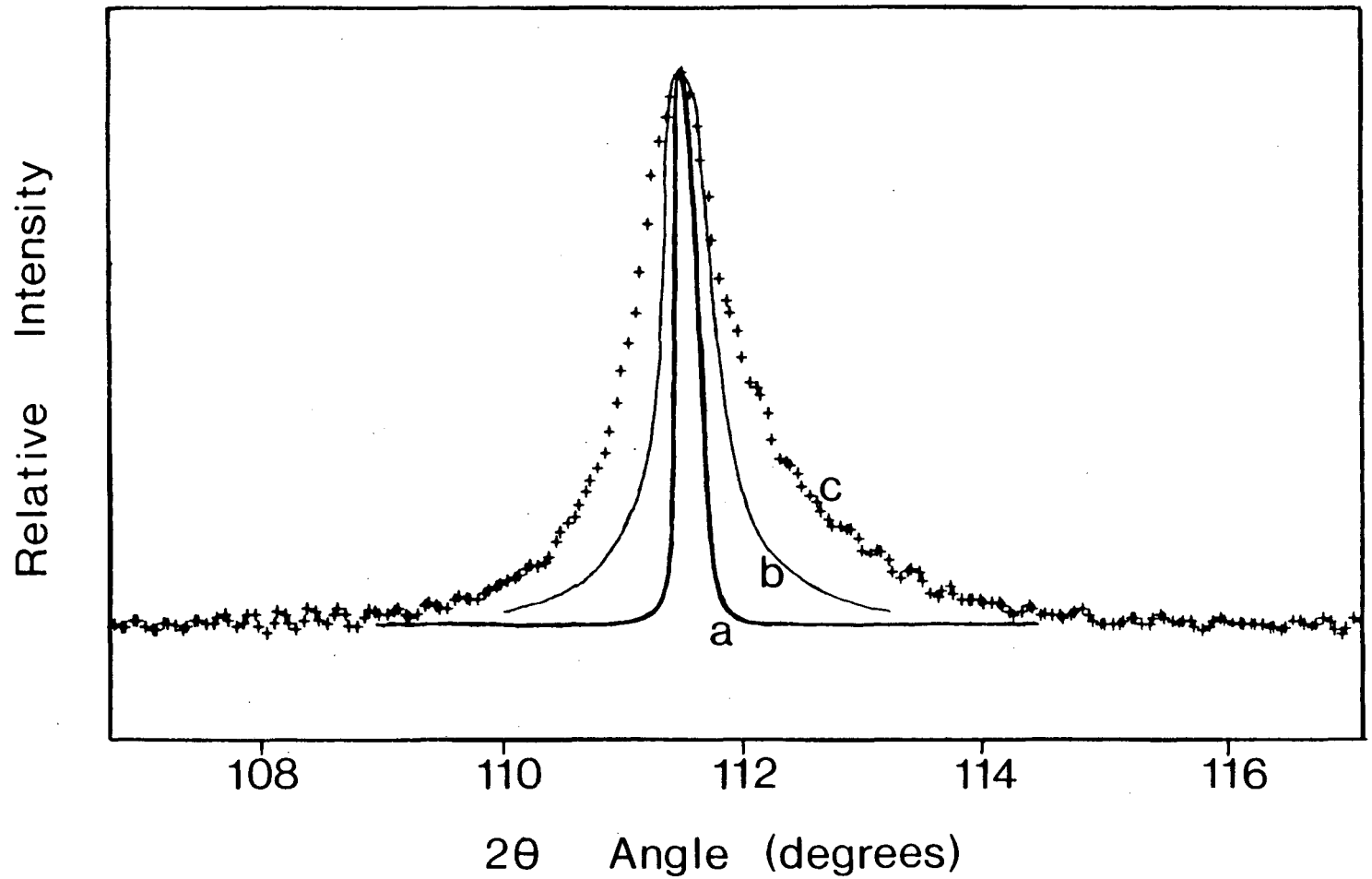

Fig. 1. Representative Rachinger and Stokes corrected (211)α' XRD peaks from 9 Ni steel. a) dark line: 9 hr tempering at 590°C, quench to 0°C. b) light line: 240 hr tempering at 590°C, quench to 0°C. c) crosses: 240 hr tempering at 590°C, quench to 0°C, 75% cold rolling.

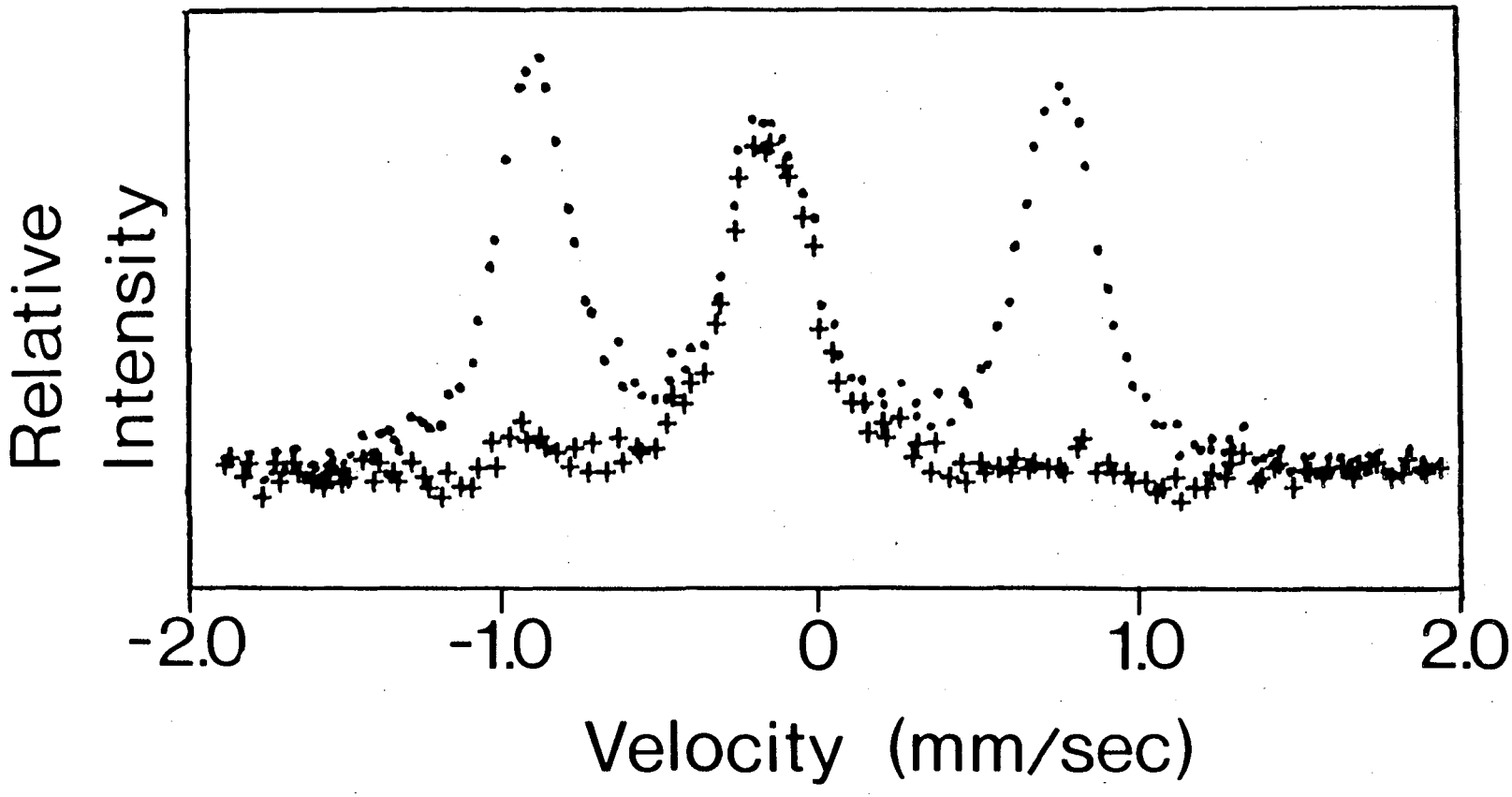

XBL 842-700

Fig. 2. Backscatter Mossbauer Spectrum of 9 Ni steel tempered 260 hrs at 590°C and immersed in liquid nitrogen. 9.0 vol.% austenite is present. Radiation source was ^{57}Co in Pd.
dots = experimental data and crosses = austenite peak corrected by stripping the adjacent martensite peaks.

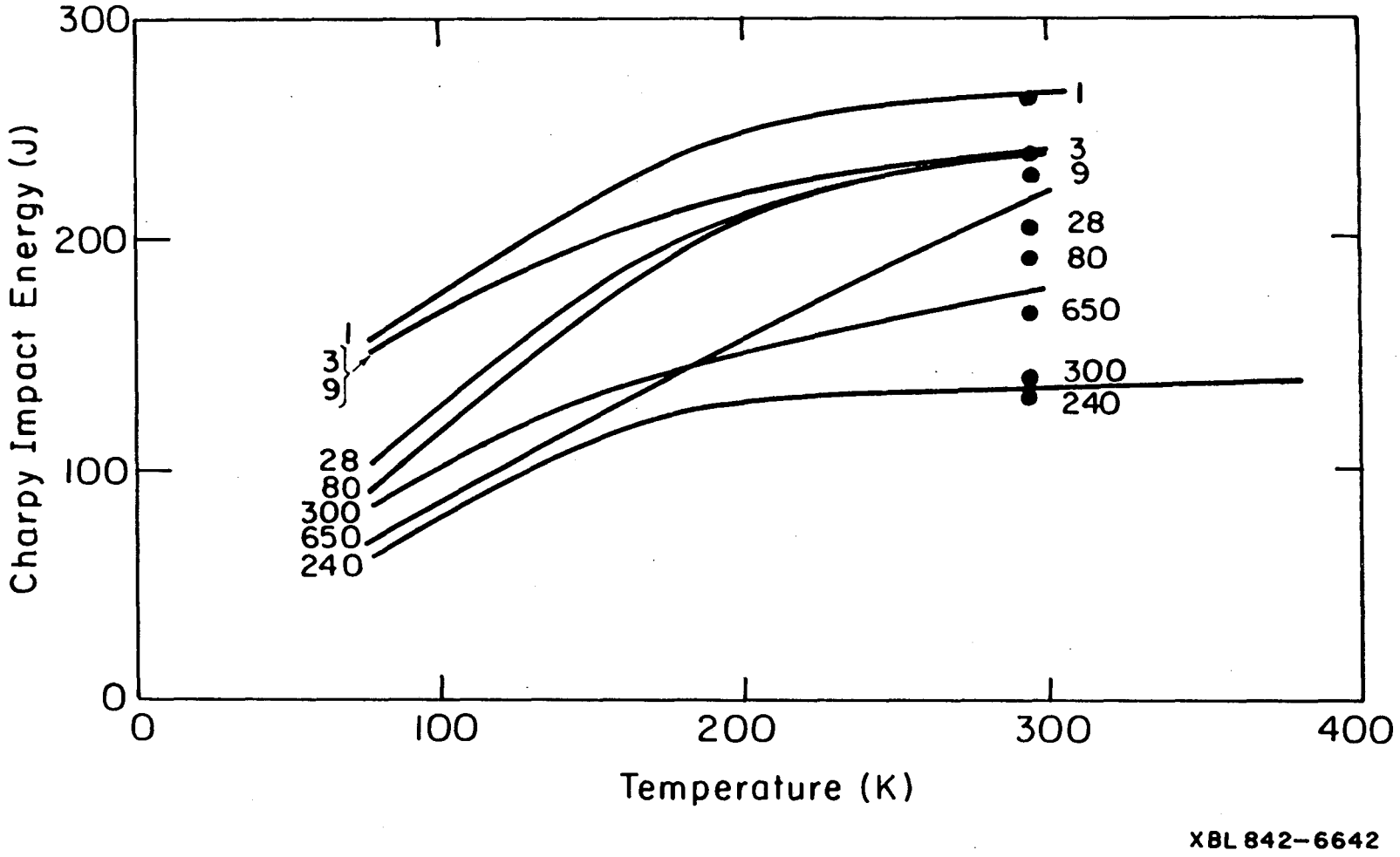

Fig. 3. Charpy impact energy versus testing temperature for 9 Ni steel tempered from 0.8 hrs to 650 hrs at 590°C. Numbers denote tempering time in hrs at 590°C. Dots denote room temperature Charpy energy after specimens were immersed in liquid nitrogen.

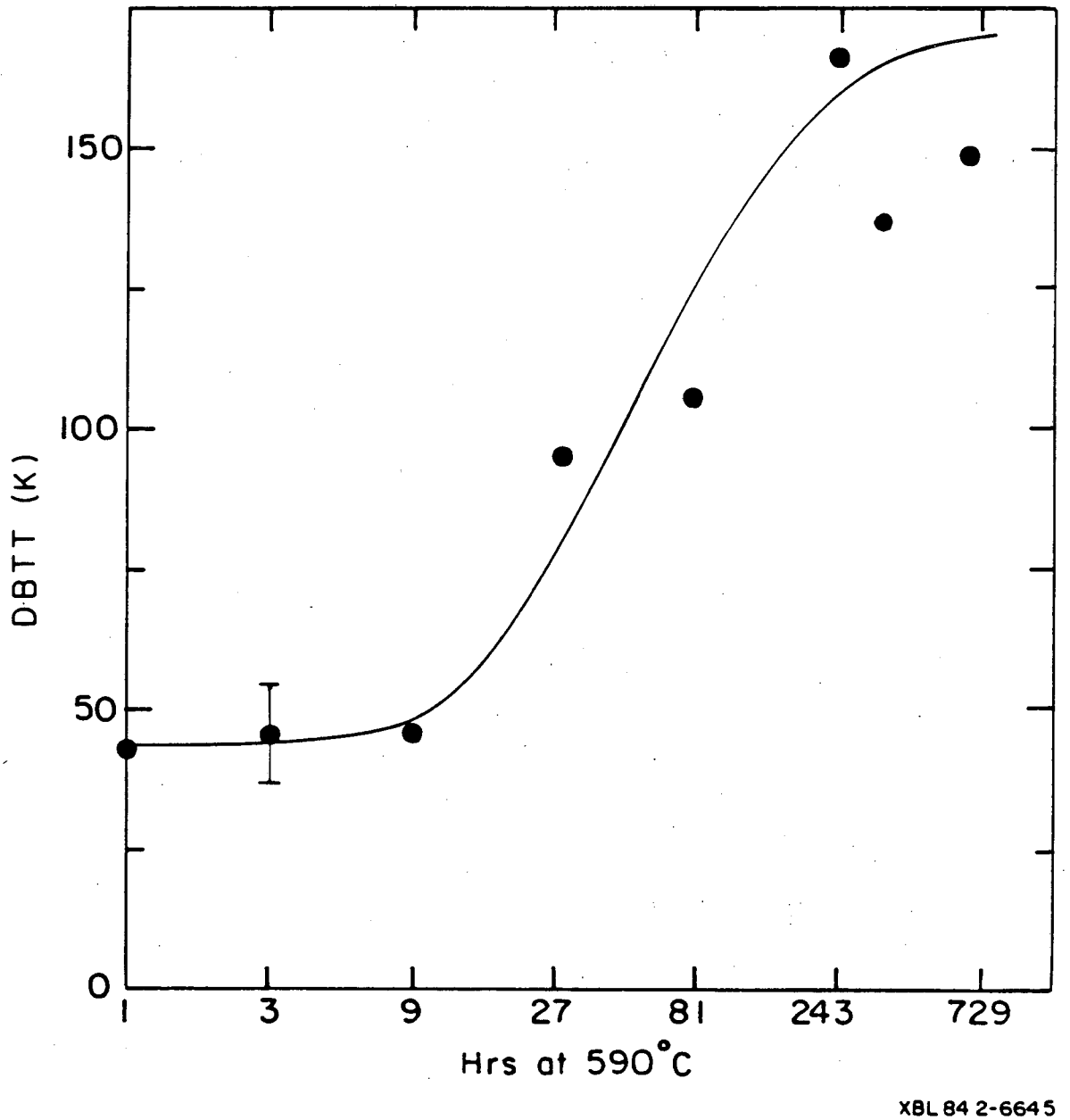

Fig. 4. Ductile-to-brittle-transition-temperature (120 J) versus tempering time at 590°C.

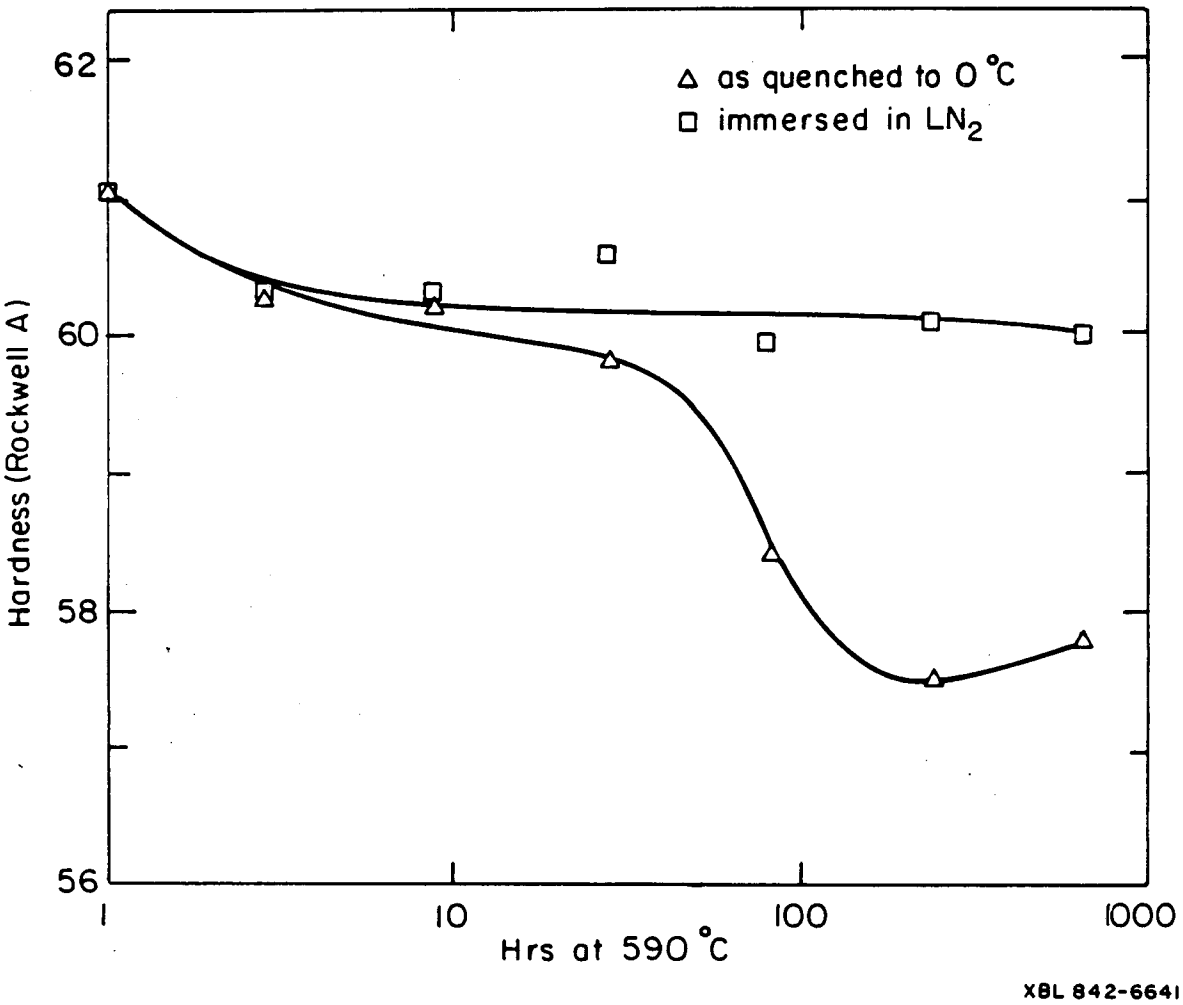

Fig. 5. Rockwell A hardness versus tempering time at 590°C. Peak up triangle: after quench to 0°C; square: after immersion in liquid nitrogen

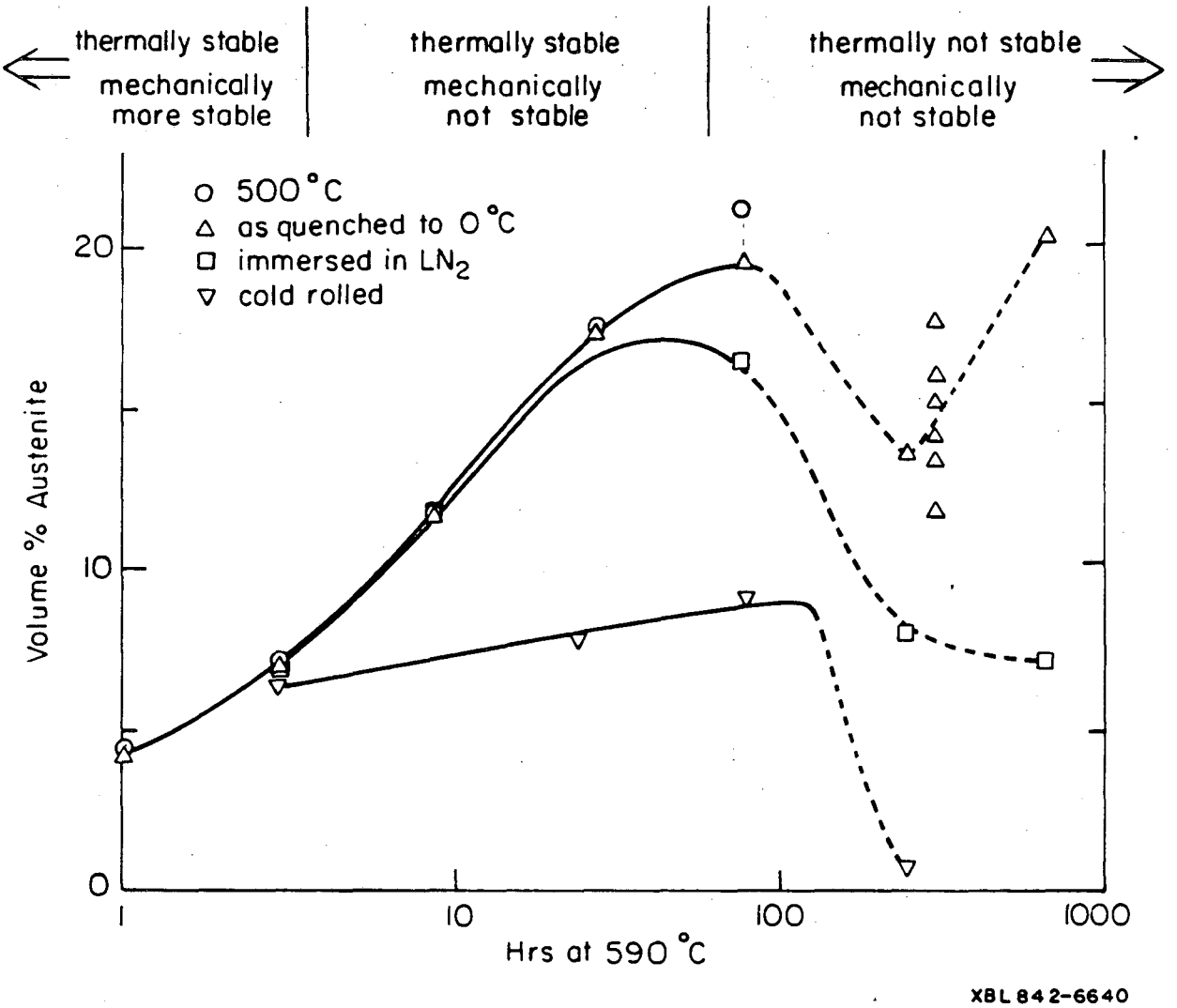

Fig. 6. Measured amount of austenite versus tempering time: peak up triangle: after quench to 0°C; square: after immersion in liquid nitrogen; peak down triangle: after 75% cold rolling; circle: increased amount at 500°C after tempering at 600°C.

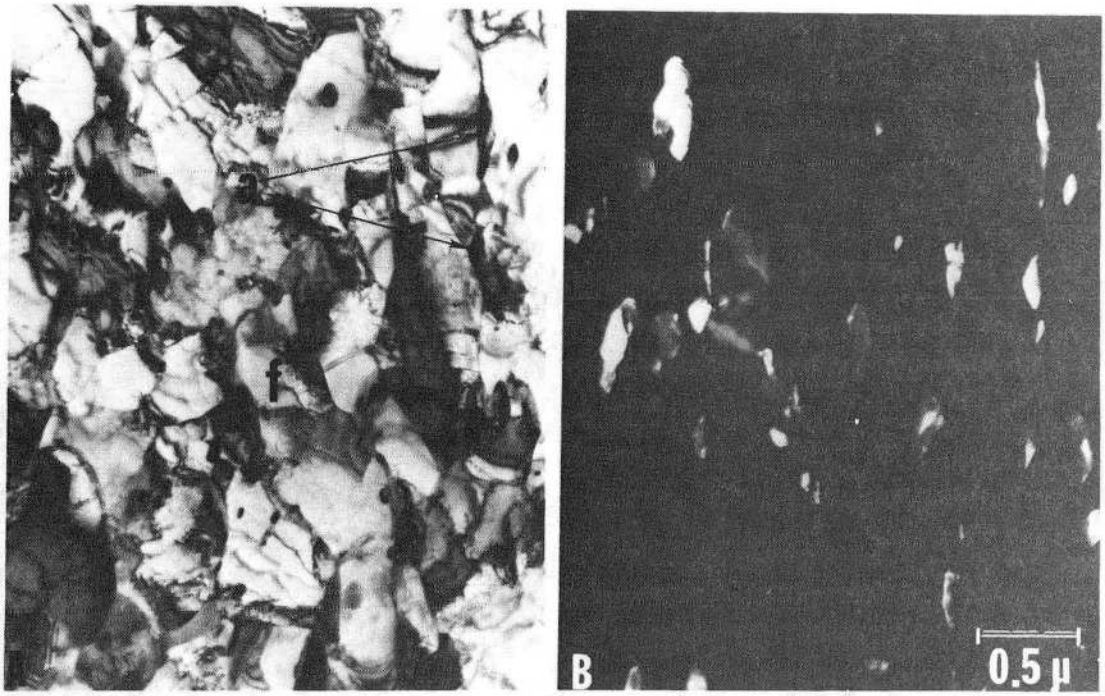

XBB 819-9181

Fig. 7. TEM micrograph of 9 Ni steel tempered 3 hrs at 590°C.
A: bright field B: dark field $00\bar{2}\gamma$.

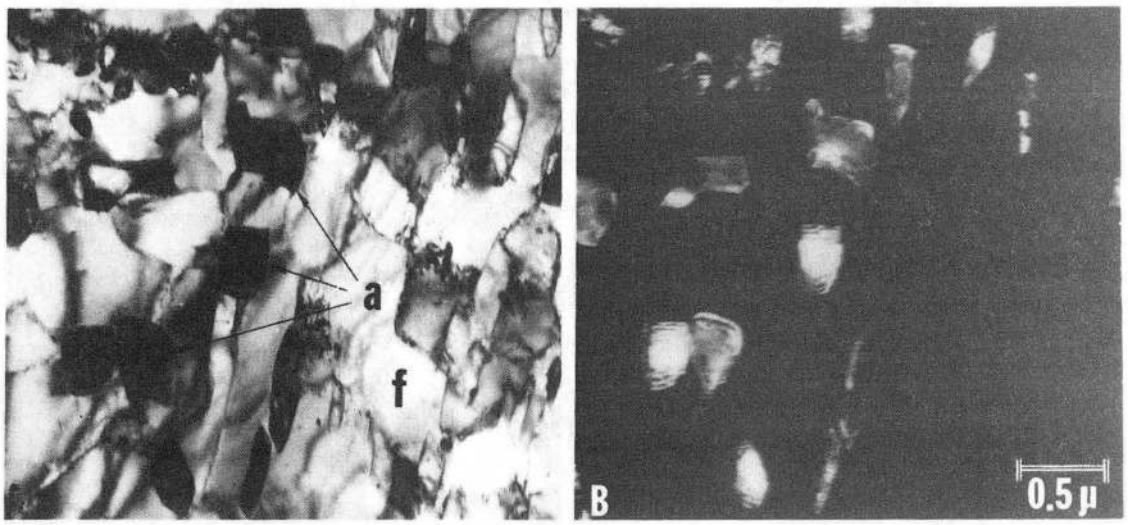

XBB 819-9184

Fig. 8. TEM micrograph of 9 Ni steel tempered 81 hrs at 590°C.
A: bright field B: dark field $00\bar{2}\gamma$.

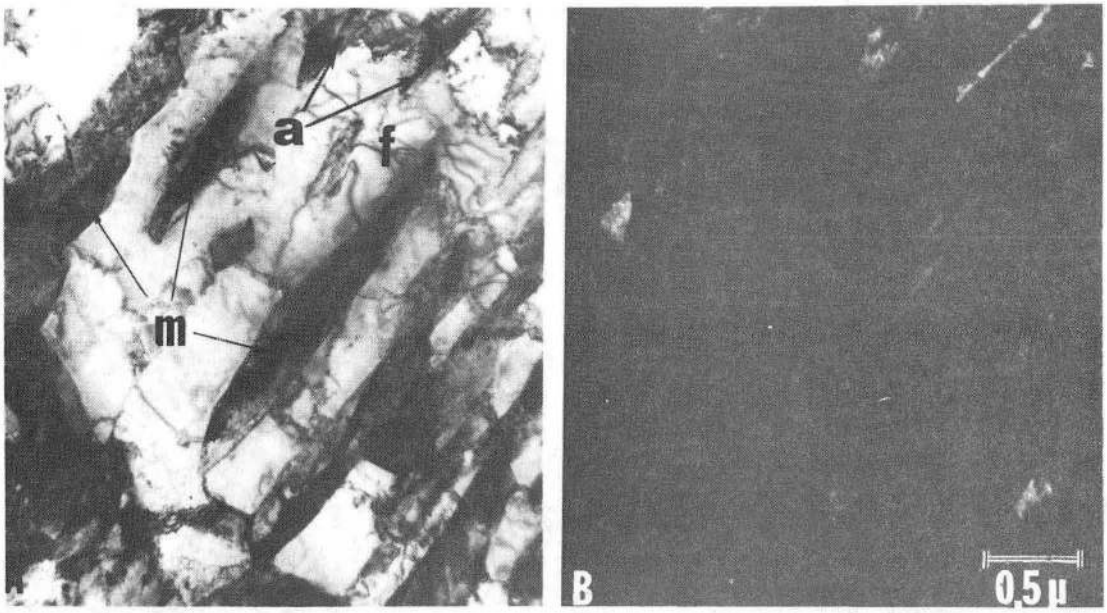

XBB 819-9182

Fig. 9. TEM micrograph of 9 Ni steel tempered 240 hrs at 590°C.
A: bright field B: dark field $00\bar{2}\gamma$.

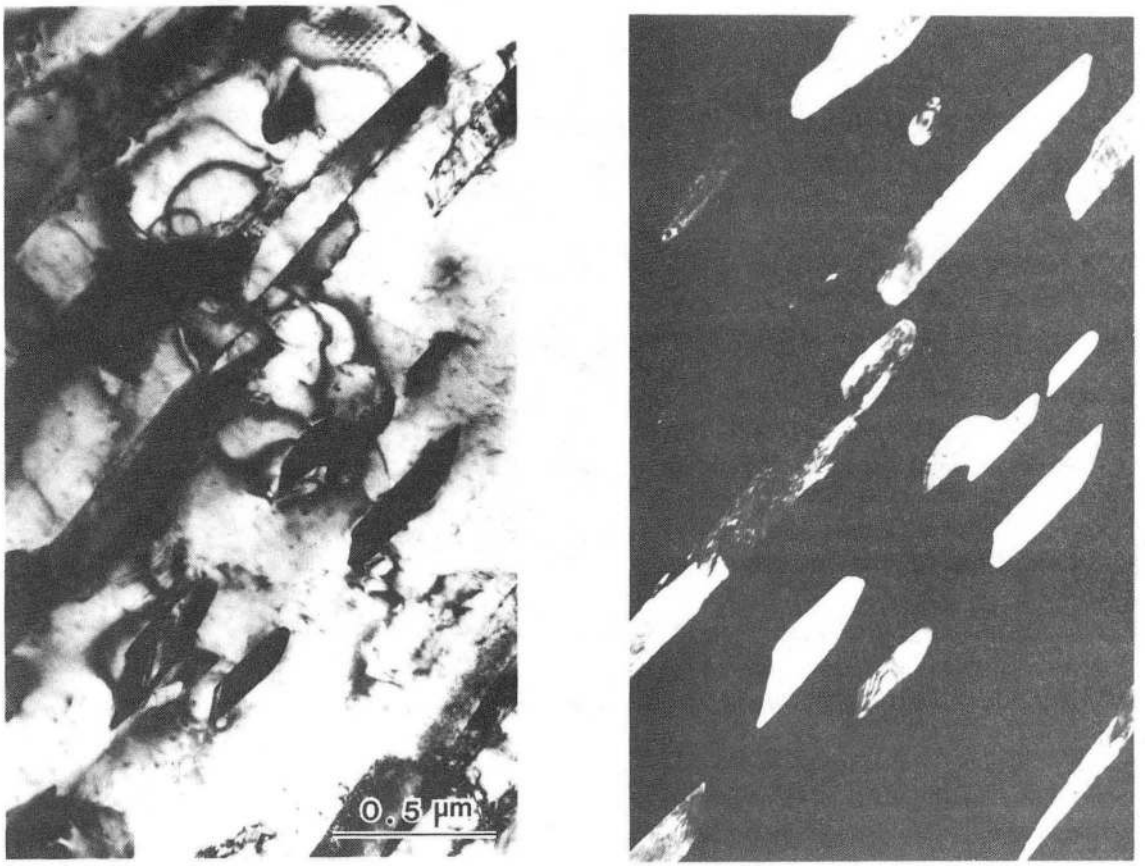

XBB 844-2631

Fig. 10. TEM micrograph of 9 Ni steel tempered 300 hrs at 590°γ.
A: bright field B: dark field of $00\bar{2}\gamma$.

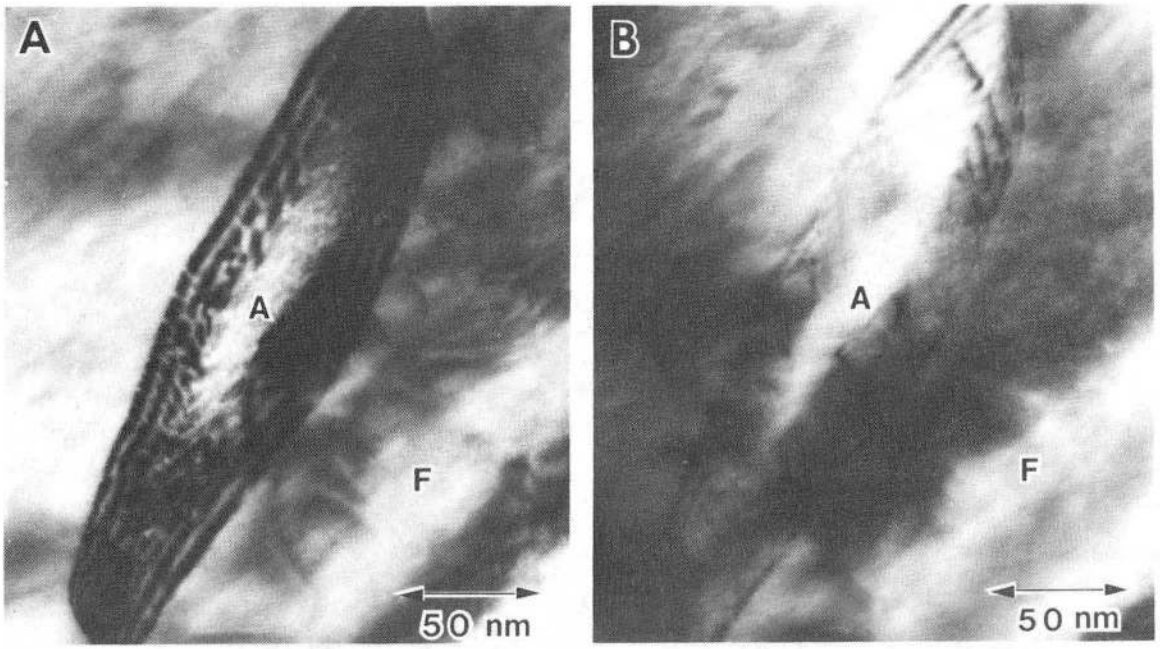

XBB 835-4182

Fig. 11. High magnification TEM micrograph of 9 Ni steel tempered 9 hrs at 590°C. A and B are both bright field micrographs taken with different contrast conditions.

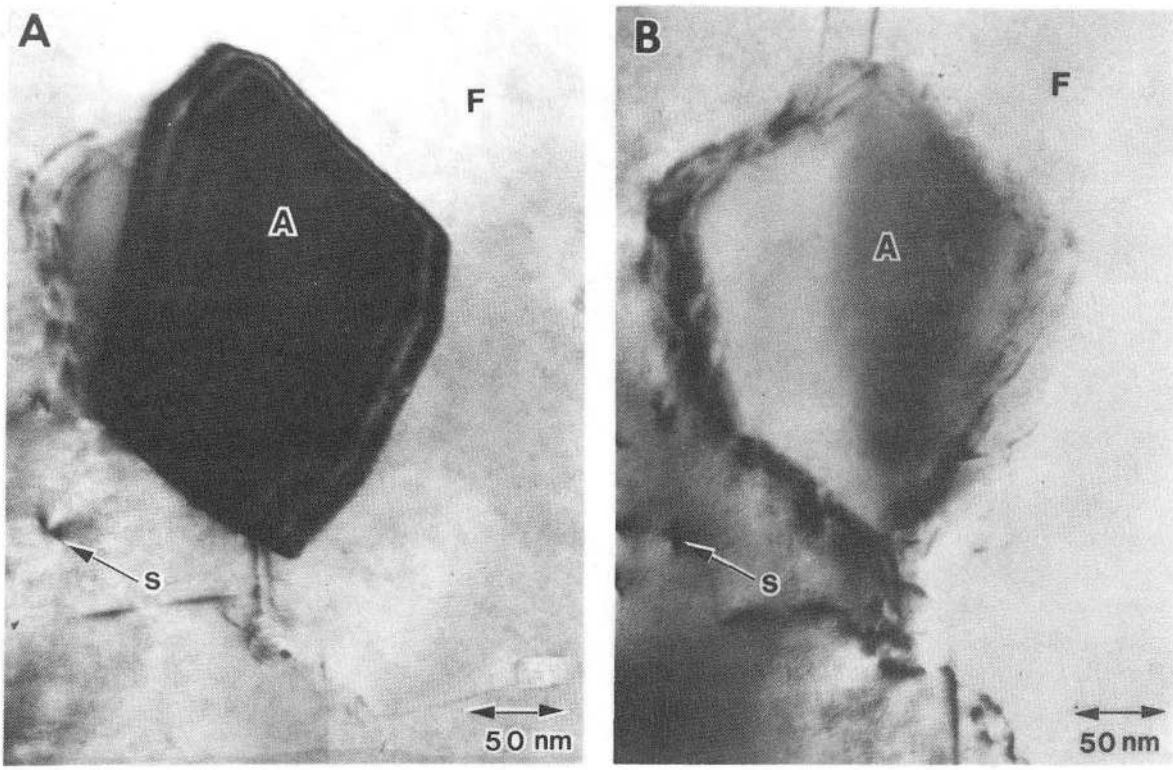

XBB 835-4185

Fig. 12. High magnification TEM micrograph of 9 Ni steel tempered 81 hrs at 590°C. A and B are both bright field micrographs taken with different contrast conditions.

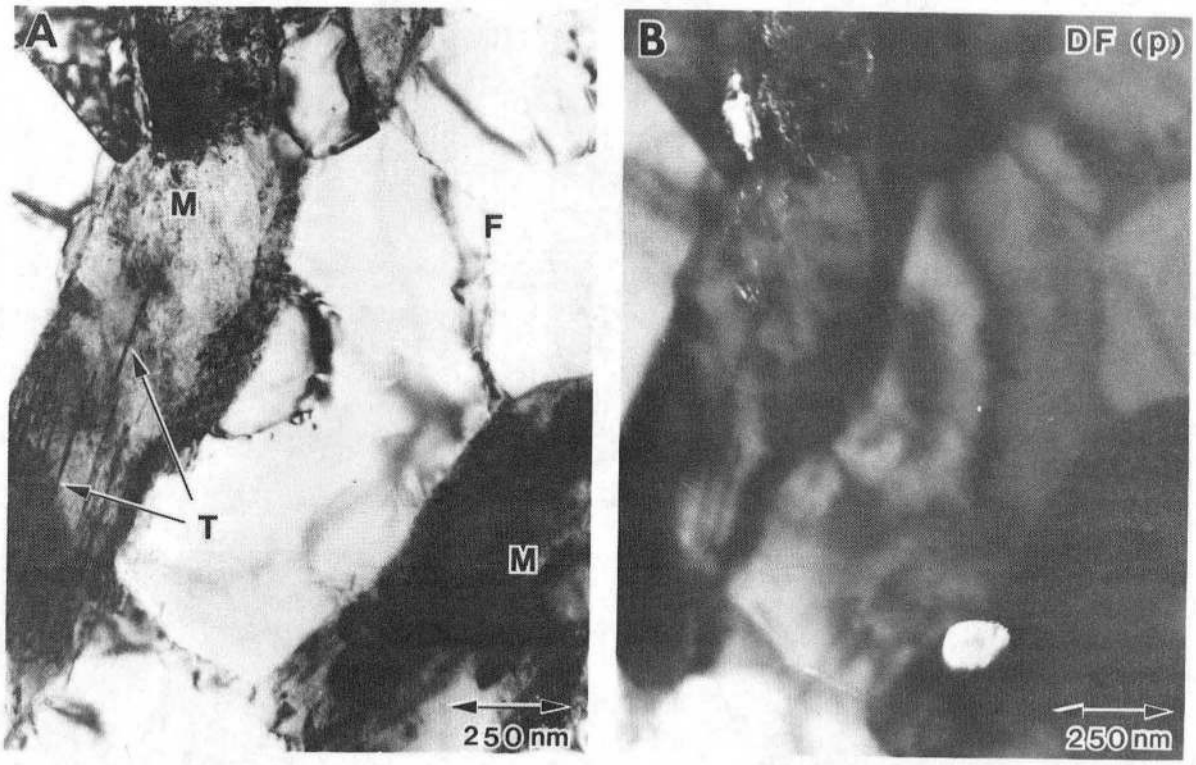

XBB 835-4183

Fig. 13. High magnification TEM micrograph of 9 Ni steel tempered 240 hrs at 590°C. A: bright field; B: dark field of (040) Fe_3C.

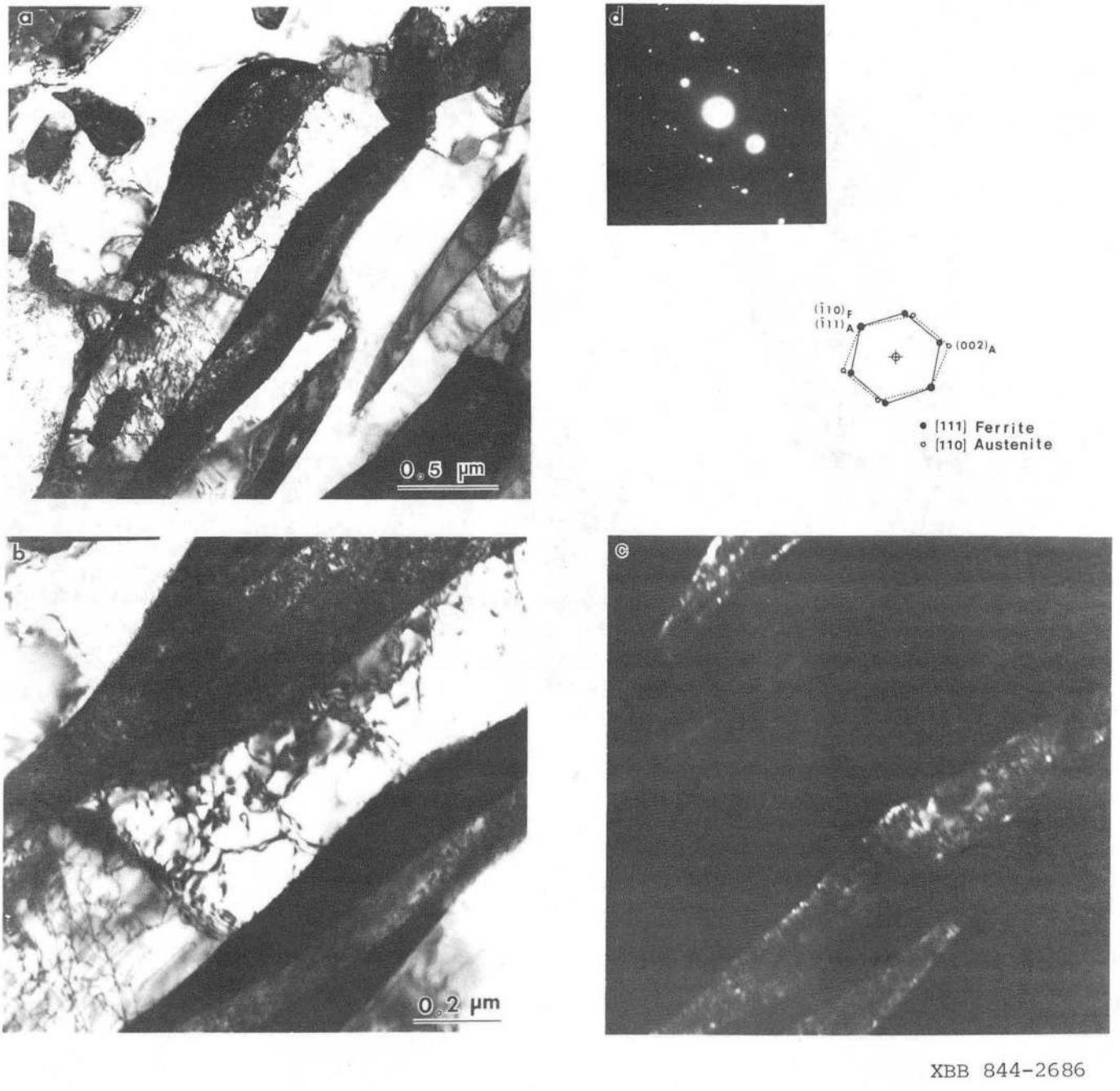

Fig. 14. TEM micrographs of 9 Ni steel tempered 300 hrs at 590°C. A: bright field; B. higher magnification bright field of central region; C: dark field of $00\bar{2}\gamma$ corresponding to B; D: indexed diffraction pattern.

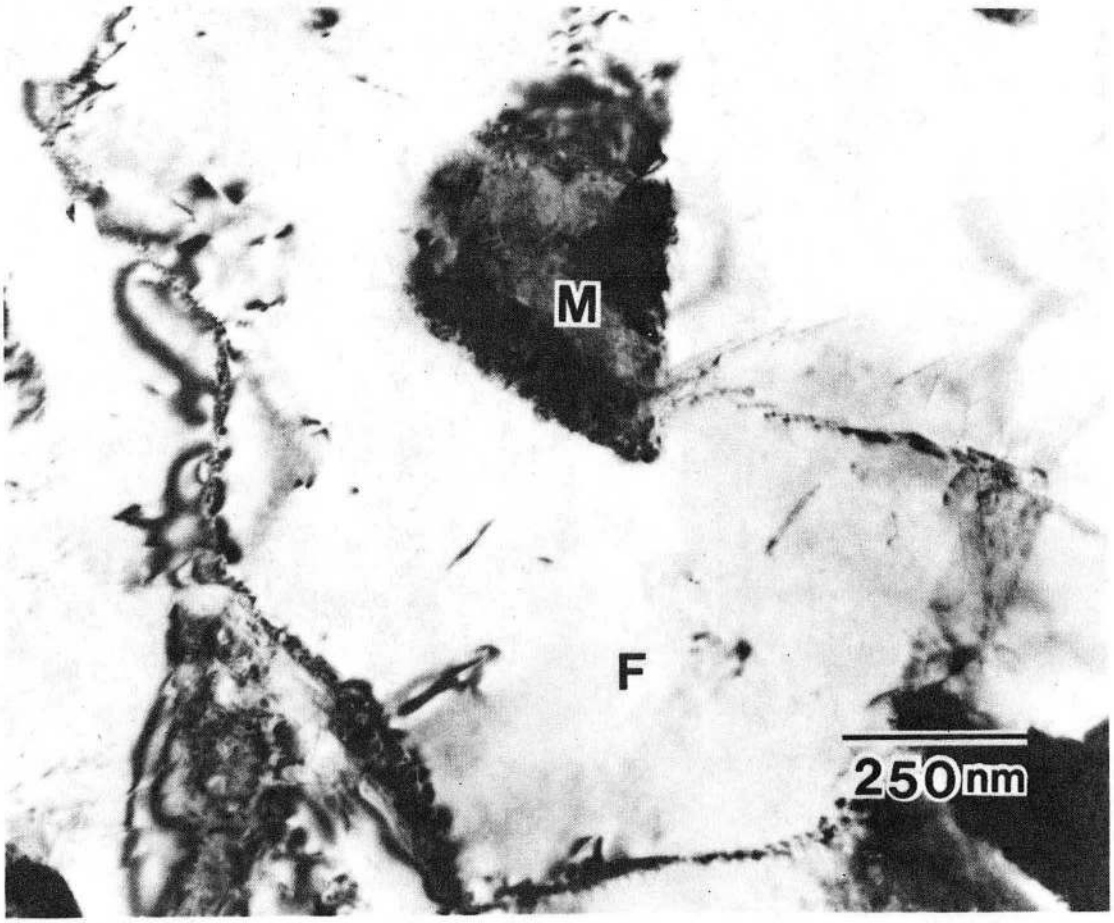

XBB 835-4181A

Fig. 15. Bright field TEM micrograph of 9Ni steel tempered 81 hrs at 590°C.

XBB 844-2630

Fig. 16. Bright field TEM micrograph of 9 Ni steel tempered hrs at 590°C followed by 25% cold rolling.

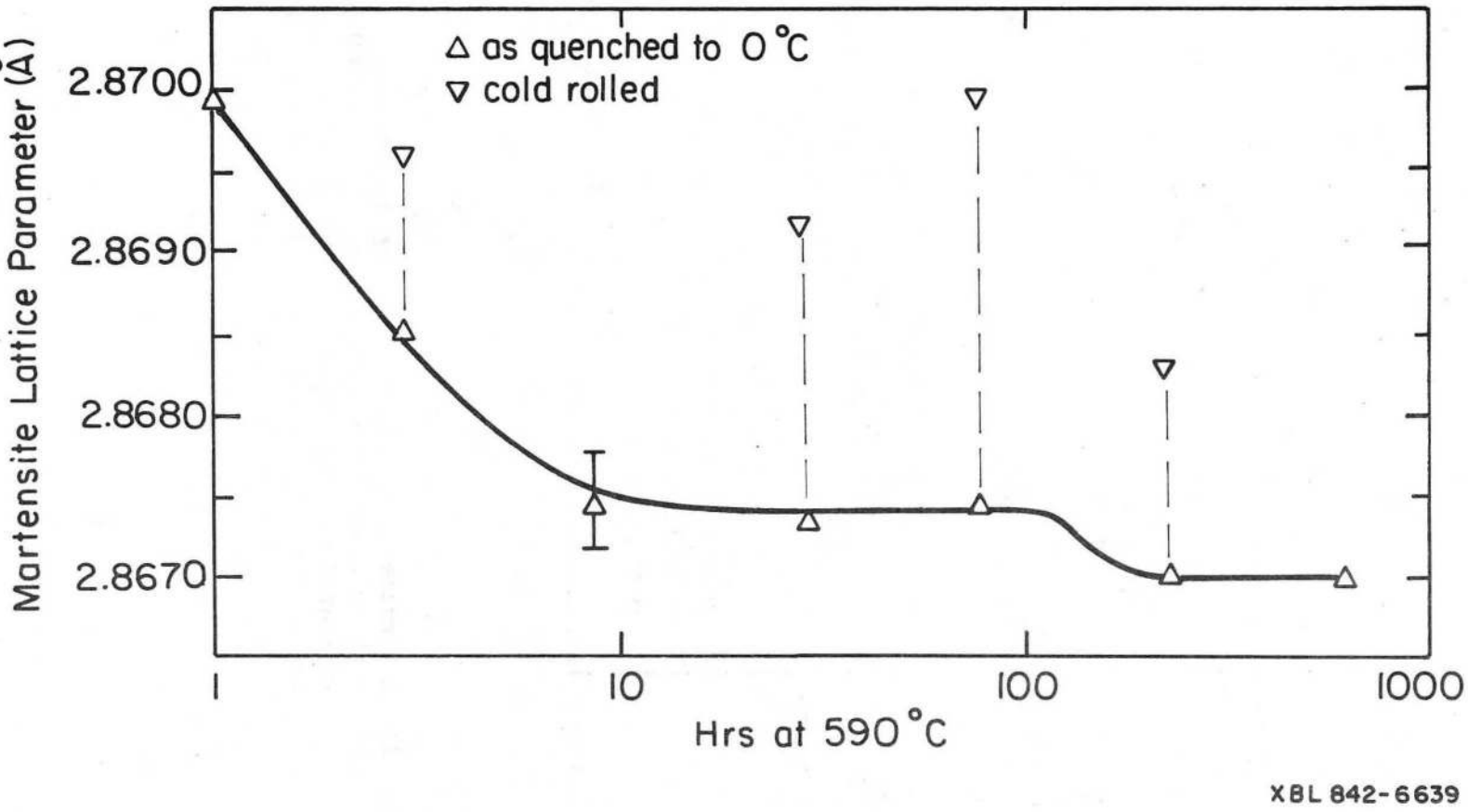

Fig. 17. Martensite lattice parameter versus tempesing time at 590°C: peak up triangle: after quench to 0°C; peak down triangle: after 75% cold rolling (four immersions in liquid nitrogen had no effect on the lattice parameter of any material).

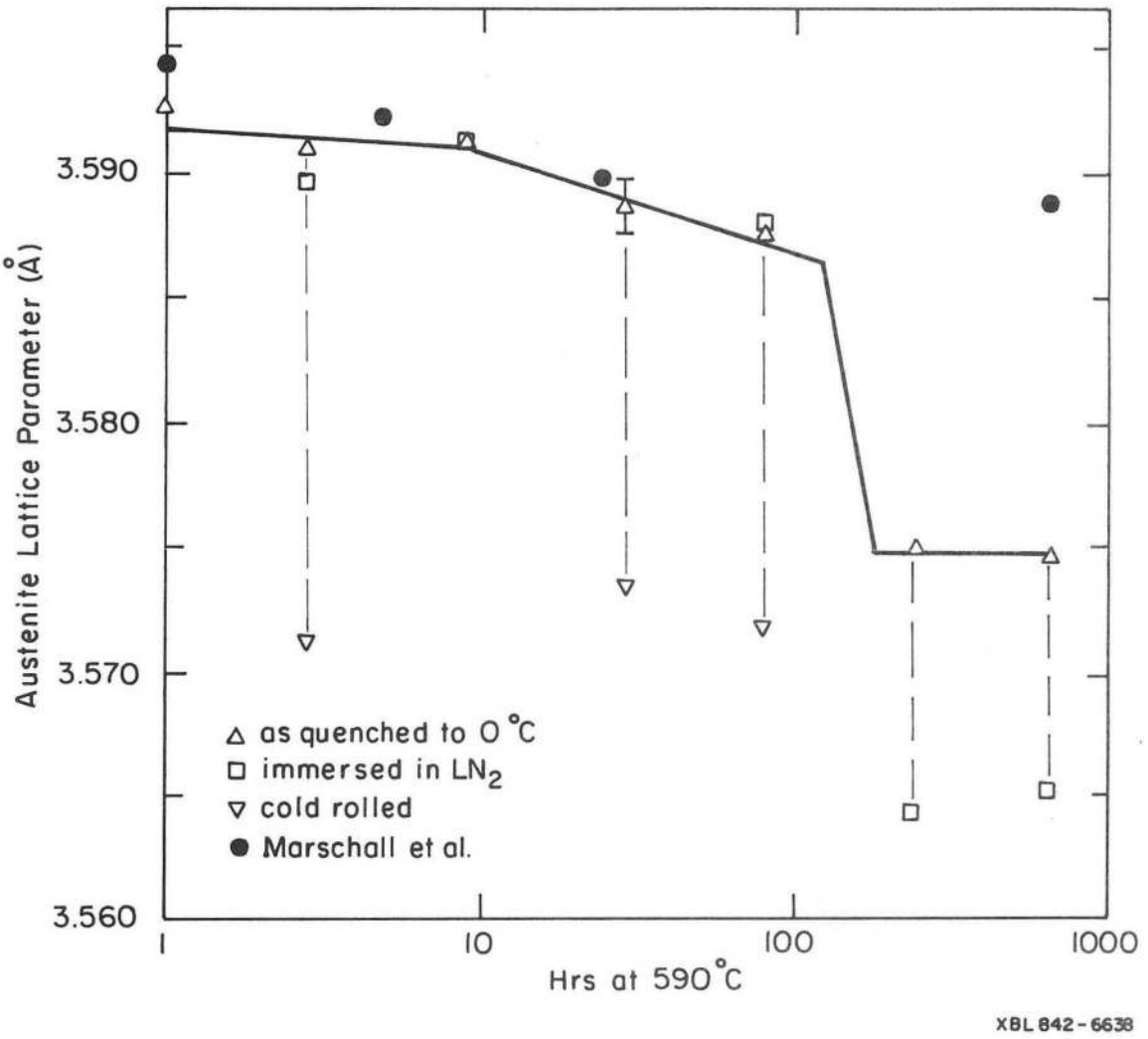

Fig. 18. Austenite lattice parameter versus tempering time at 590°C: peak up triangle: after quench to 0°C; square: after immersion in liquid nitrogen; peak down triangle: after 75% cold rolling; solid circle: data from Marschall, et al. [7]

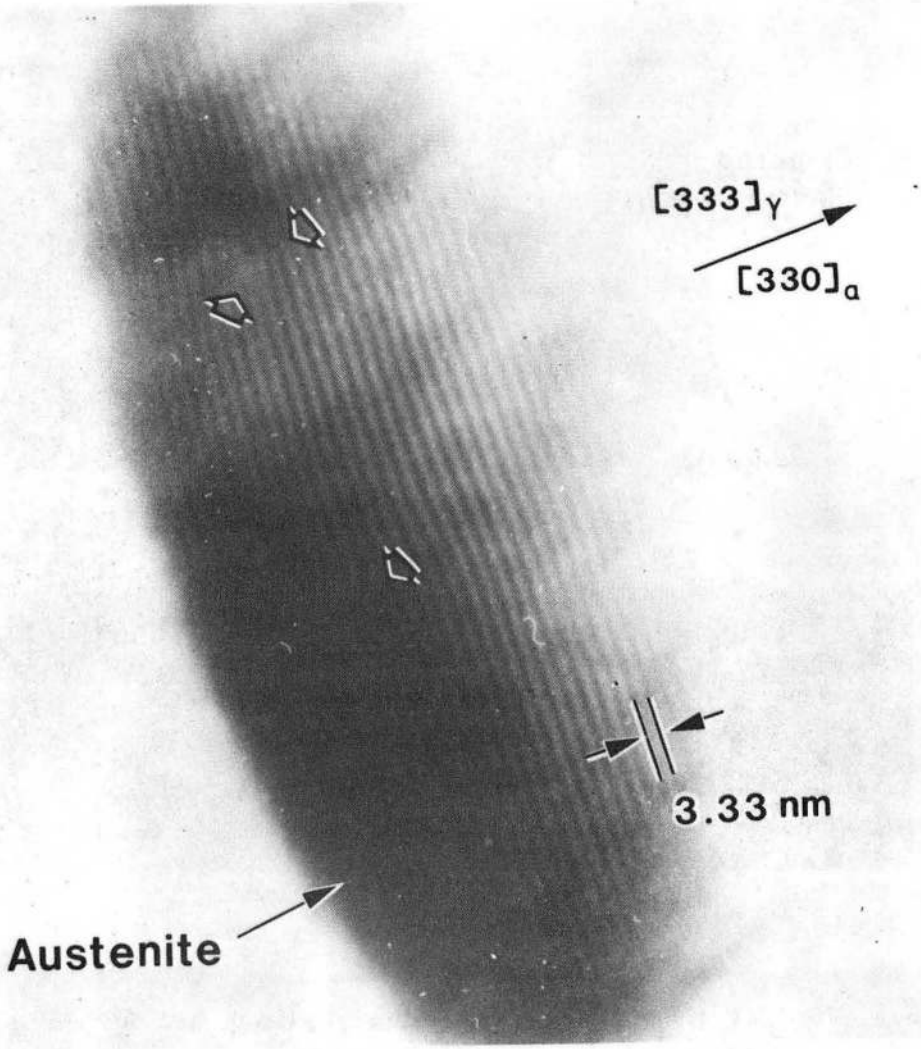

XBB 844-2989

Fig. 19. Bright field Moiré fringes from 9 hr tempered material using strongly operating 333γ and 330α′ diffractions. Terminating (333)γ or (330)α′ planes are indicated by the open arrows.

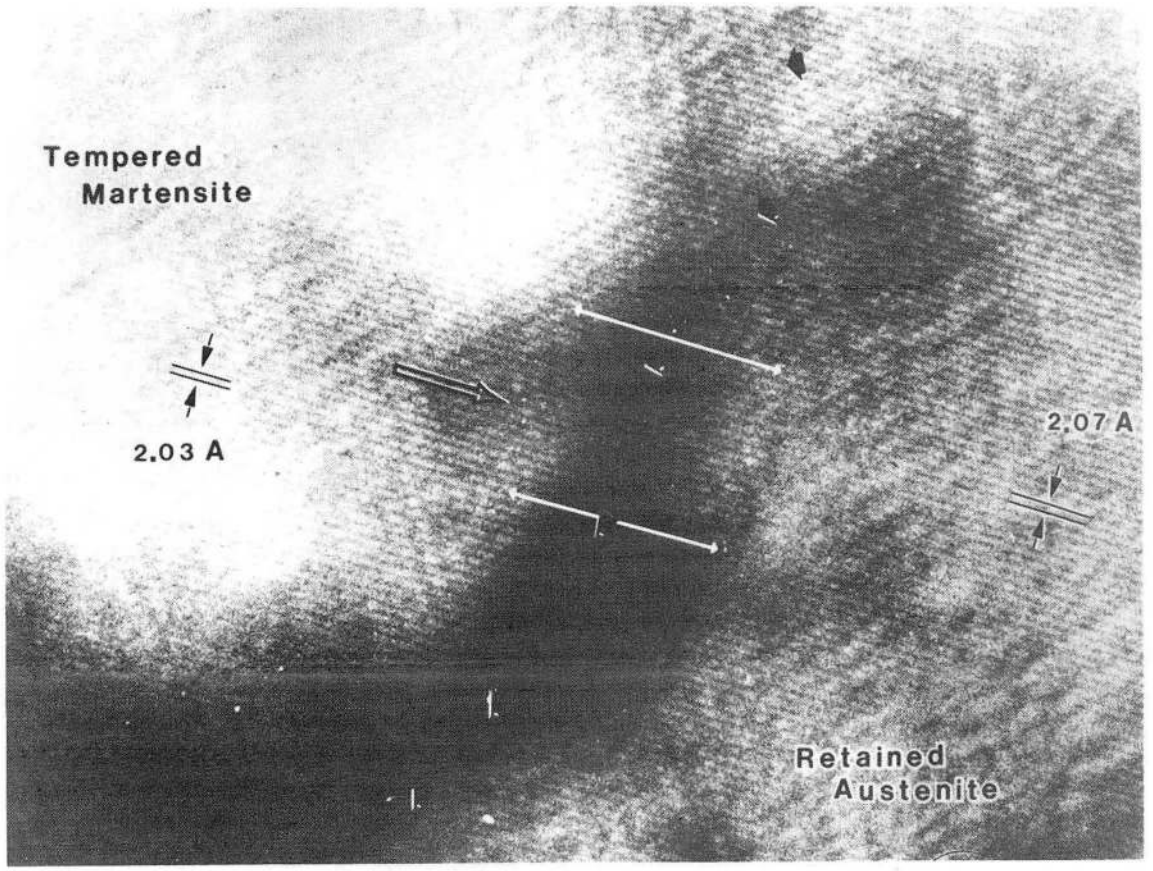

XBB 844-2990

Fig. 20. Lattice fringes from (111)γ planes and (110)α' planes across the austenite/martensite interface of 3 hr tempered material. The interface is indicated by the dark arrows. An unmatched (110)α' plane is indicated by the open arrow.

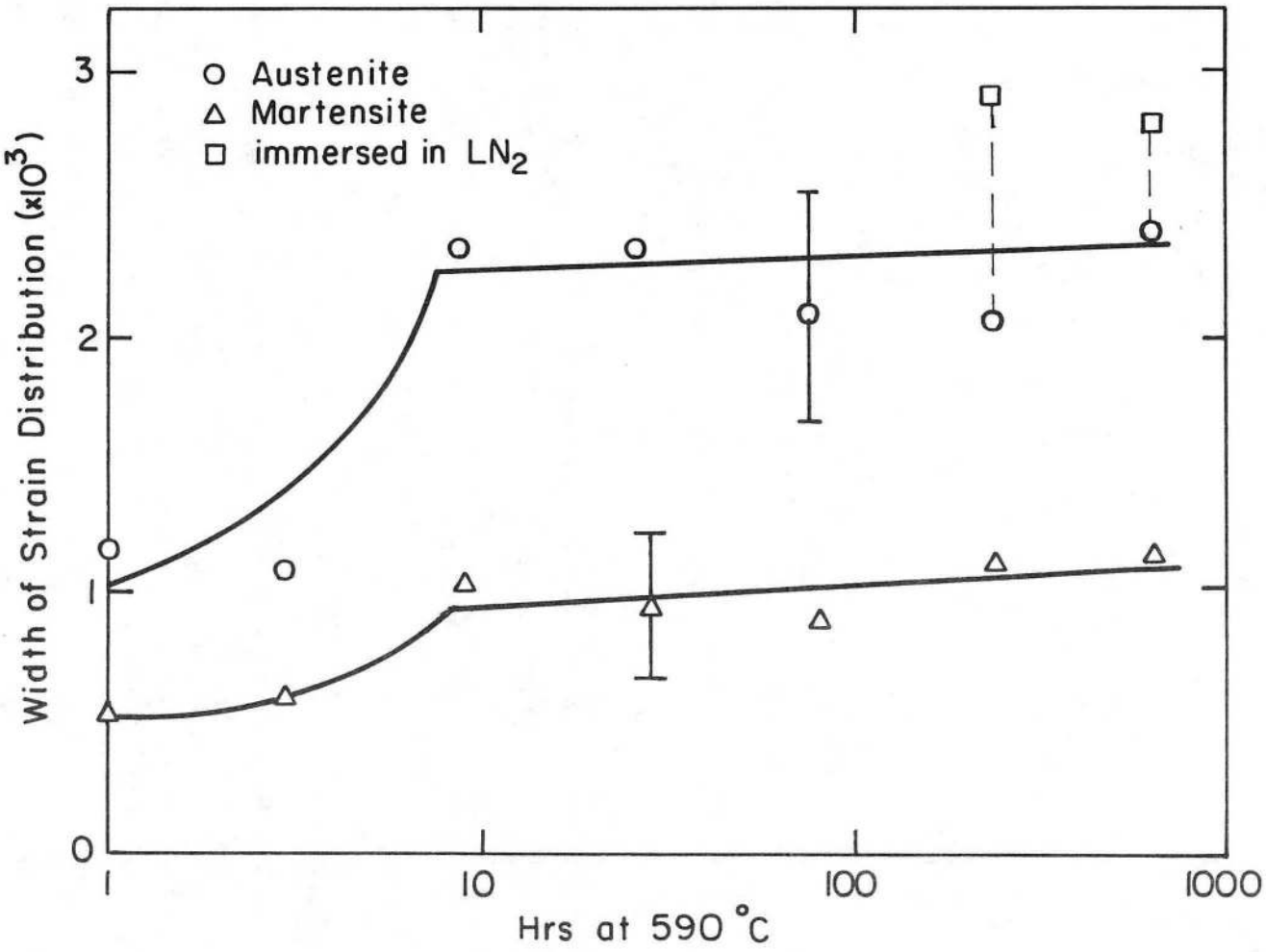

XBL 842-6644

Fig. 21. Full-width-at-half-maximum of the strain distribution versus tempering time at 590°C. Circle: austenite; peak up triangle: martensite; square: austenite immersed in liquid nitrogen.

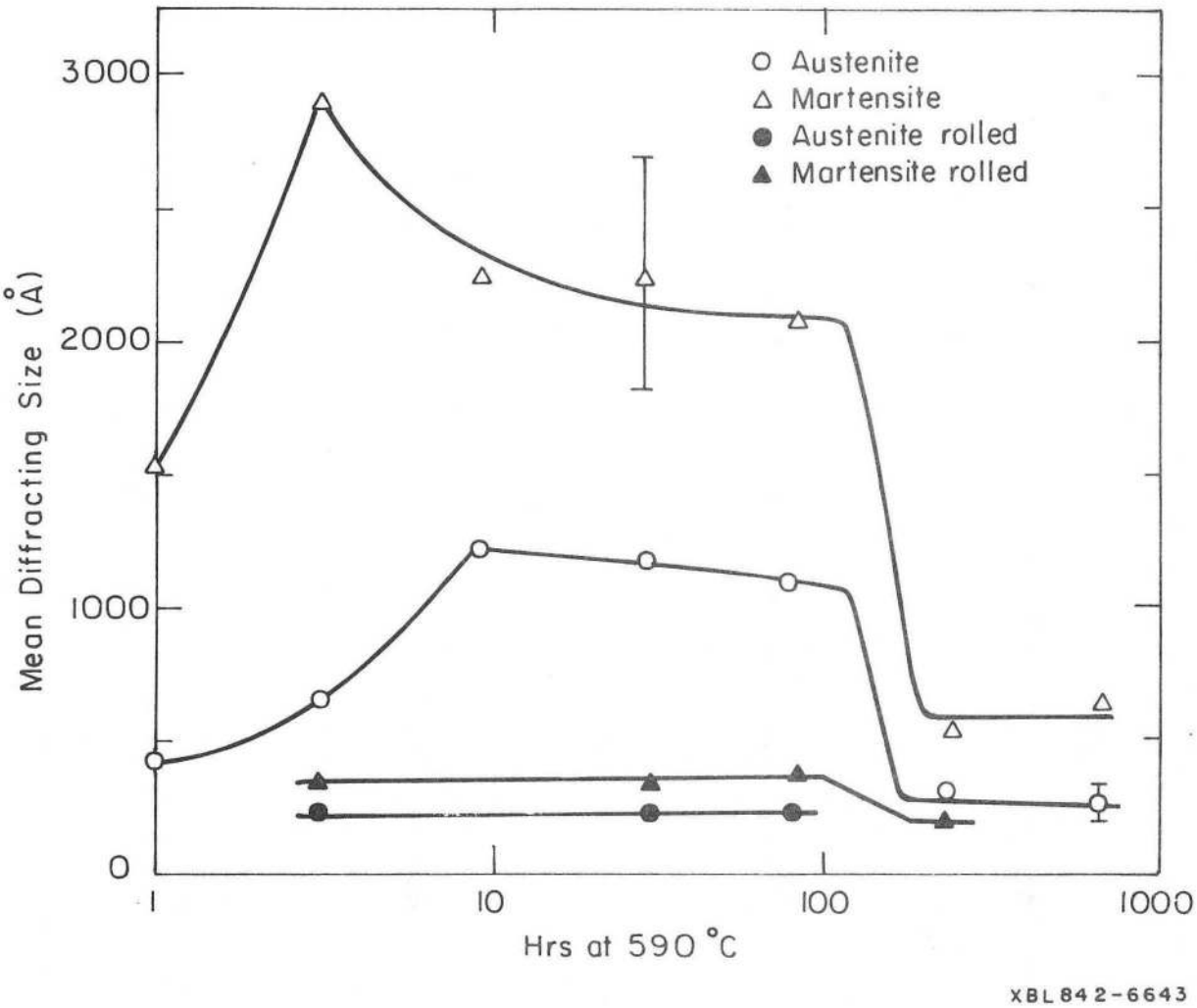

Fig. 22. Mean size of coherently diffracting domains versus tempering time at 590°C. Circle: austenite quenched to 0°Cμ triangle: martensite quenched to 0°C; solid circle: austenite after 75% cold rolling; solid triangle: martensite after 75% cold rolling.

This report was done with support from the Department of Energy. Any conclusions or opinions expressed in this report represent solely those of the author(s) and not necessarily those of The Regents of the University of California, the Lawrence Berkeley Laboratory or the Department of Energy.

Reference to a company or product name does not imply approval or recommendation of the product by the University of California or the U.S. Department of Energy to the exclusion of others that may be suitable.

TECHNICAL INFORMATION DEPARTMENT
LAWRENCE BERKELEY LABORATORY
UNIVERSITY OF CALIFORNIA
BERKELEY, CALIFORNIA 94720